Motion between the Indian, Antarctic and African plates in the early Cenozoic

Steven C Cande, Philippe Patriat, Jerome Dyment

Geophysical Journal International

Geophys. J. Int. (2010) **183,** 127–149 doi: 10.1111/j.1365-246X.2010.04737.x

Motion between the Indian, Antarctic and African plates in the early Cenozoic

Steven C. Cande,[1] Philippe Patriat[2] and Jerome Dyment[2]

[1] *Scripps Institution of Oceanography, La Jolla, CA, USA. E-mail: scande@ucsd.edu*

[2] *Laboratoire de Geosciences Marines, Institut de Physique du Globe de Paris,* 4 *place Jussieu,* 75252 *Paris Cedex* 05*, France*

Accepted 2010 July 14. Received 2010 July 9; in original form 2010 April 29

SUMMARY

We used a three-plate best-fit algorithm to calculate four sets of Euler rotations for motion between the India (Capricorn), Africa (Somali) and Antarctic plates for 14 time intervals in the early Cenozoic. Each set of rotations had a different combination of data constraints. The first set of rotations used a basic set of magnetic anomaly picks on the Central Indian Ridge (CIR), Southeast Indian Ridge (SEIR) and Southwest Indian Ridge (SWIR) and fracture zone constraints on the CIR and SEIR, but did not incorporate data from the Carlsberg Ridge and did not use fracture zones on the SWIR. The second set added fracture zone constraints from the region of the Bain fracture zone on the SWIR which were dated with synthetic flowlines based on the first data set. The third set of rotations used the basic constraints from the first rotation set and added data from the Carlsberg Ridge. The fourth set of rotations combined both the SWIR fracture zone constraints and the Carlsberg Ridge constraints. Data on the Indian Plate side of the Carlsberg Ridge (Arabian Basin) were rotated to the Capricorn Plate before being included in the constraints. Plate trajectories and spreading rate histories for the CIR and SWIR based on the new rotations document the major early Cenozoic changes in plate motion. On the CIR and SEIR there was a large but gradual slowdown starting around Chron 23o (51.9 Ma) and continuing until Chron 21y (45.3 Ma) followed 2 or 3 Myr later by an abrupt change in spreading azimuth which started around Chron 20o (42.8) Ma and which was completed by Chron 20y (41.5 Ma). No change in spreading rate accompanied the abrupt change in spreading direction. On the SWIR there was a continuous increase in spreading rates between Chrons 23o and 20o and large changes in azimuth around Chrons 24 and 23 and again at Chron 21. Unexpectedly, we found that the two sets of rotations constrained by the Carlsberg Ridge data diverged from the other two sets of rotations prior to anomaly 22o. When compared to rotations for the CIR that are simultaneously constrained by data from all three branches of the Indian Ocean Triple Junction, there is a progressively larger separation of anomalies on the Carlsberg Ridge, with a roughly 25 km misfit for anomaly 23o and increasing to over 100 km for anomaly 26y. These data require that there was previously unrecognized convergence somewhere in the plate circuit linking the Indian, Capricorn and Somali plates prior to Chron 22o. We quantify this motion by summing our new Capricorn–Somalia rotations with previously published rotations for Neogene India–Capricorn motion and for early Cenozoic Somali–India motion based solely on Carlsberg Ridge data. The most likely possibility is that there was motion within the Somalia Plate due to a distinct Seychelles microplate as young as Chron 22o. The sense of the misfit on the Carlsberg Ridge is consistent with roughly 100–150 km of convergence across a boundary passing through the Amirante Trench and extending north to the Carlsberg Ridge axis between anomalies 26y and 22o. Alternatively, there may have been convergence within the Indian Plate, either along the western margin of Indian or east of the CIR in the region of the current Capricorn–Indian diffuse plate boundary. Our work sharpens the dating of the two major Eocene changes in plate motion recognized in the Indian Ocean.

Key words: Plate motions; Kinematics of crustal and mantle deformation; Indian Ocean.

INTRODUCTION

Knowledge of plate motions in the Indian Ocean has evolved over the last four decades, beginning with the studies that initially incorporated marine geophysical constraints (Bergh 1971; McKenzie & Sclater 1971; Sclater & Fisher 1974; Schlich 1975; Bergh & Norton 1976; Norton & Sclater 1979; Schlich 1982), to the comprehensive studies of Patriat (1987), Patriat & Achache (1984) and Dyment (1993) that portrayed the development of the Indian Ocean Triple Junction (IOTJ) in great detail. Molnar *et al*. (1988) made an important contribution with the introduction of quantitative estimates of uncertainties in the Euler rotations. The development of gravity fields based on satellite altimetry measurements (Haxby 1987; Sandwell & Smith 1997), with the consequent ability to map fracture zones in remote areas, led to a further improvement in plate reconstructions (Royer *et al*. 1988; Royer & Sandwell 1989; Nankivell 1997; Bernard *et al*. 2005).

Problems still exist in our knowledge of Indian Ocean Plate motions in the Early Cenozoic. The details of the dramatic slowdown in the northward motion of the Indian Plate around Chron 22 (50 Ma; all ages are from the magnetic polarity timescale of Gradstein *et al*. 2004) and the abrupt change in direction around Chron 20 (42 Ma) correlated, respectively, with the 'soft' and 'hard' collision of India with Eurasia (Patriat & Achache 1984), are still not clear. Events in other parts of the Indian Ocean are also not well known. For example, spreading in the Mascarene Basin ceased around Chron 27 (61 Ma) (Dyment 1991) following the onset of rifting between the Seychelles–Mascarene Ridge and the west coast of India, but it is not known how quickly this process took place. It has been speculated (Plummer 1996; Dyment 1998) that both the Mascarene Ridge and Carlsberg Ridge were active simultaneously for a while and that during this time there was a distinct Seychelles microplate.

Other complexities in studying the Indian Ocean are related to crustal deformation in the Central Indian Ocean between the Indian and Australian plates (Wiens *et al*. 1985), the recognition of the Capricorn Plate, the region south of the zone of deformation in the Central Indian Ocean and west of the Ninety-East Ridge, as a separate entity from the rest of the Australian Plate (Royer & Gordon 1997), and the proposal that the African Plate has also behaved as two or three distinct plates (Lemaux *et al*. 2002; Horner-Johnson *et al*. 2007). Incomplete knowledge of when deformation started and how long it lasted in the various regions, introduces uncertainty in the calculation of Euler rotations.

Another problem in improving reconstructions, has been ambiguities in the mapping of fracture zones on the Southwest Indian Ridge (SWIR) where very slow spreading rates and large changes in spreading direction led to complex topographic signatures (Patriat *et al*. 1985; Royer *et al*. 1988; Bernard *et al*. 2005). The sparsity of shipboard surveys on the older flanks of the SWIR means that there are often no magnetics data to control the age offsets on these fracture zones in the early Cenozoic.

These problems can be addressed with quantitative methods that solve for the motion between three plates simultaneously. Because of the larger number of constraints involved, three-plate solutions generally are more informative than two-plate solutions and it is possible, for example, to test the effect of omitting various pieces of suspect data. In this paper we apply the statistical methods of Chang (1987, 1988) and Royer & Chang (1991) as applied to three-plate situations by Kirkwood *et al*. (1999) to the calculation of finite rotation parameters on the three branches of the Central IOTJ for 14 Early Cenozoic magnetic anomalies. The rotations are closely spaced in time so that changes in plate motions can be more accurately portrayed than in previous studies. The solutions were run using four combinations of data: with and without constraints from the Carlsberg Ridge and with and without constraints from the fracture zones on the SWIR, so that potential problems arising from combining these various geophysical constraints could be evaluated. We found that the Carlsberg Ridge was not opening in concert with the Somalia and India (Capricorn) plates prior to Chron 22o, indicating that there was a previously unrecognized period of convergence somewhere in the plate circuit linking the Indian, Capricorn and Somali plates at this time. The three-plate solutions tightly portray the dramatic slowdown and change in spreading direction in the Indian Ocean in the early Cenozoic and we present revised trajectories for the motion of Capricorn with respect to Somalia and Antarctica, and Somalia with respect to Antarctica.

BACKGROUND

The basic tectonic evolution of the Indian Ocean since the breakup of Gondwanaland in the Jurassic was laid out in a classic paper by McKenzie & Sclater (1971). The spreading history was further developed in a series of papers in the 1970s by Bergh (1971), Fisher *et al*. (1971), Sclater & Fisher (1974), Schlich (1975), Bergh & Norton (1976) and Norton & Sclater (1979). These papers described the tectonic evolution in large time steps—for example, Norton & Sclater (1979) presented Cenozoic and Late Cretaceous reconstructions for Chrons 16, 22, 29 and 34. A landmark paper by Patriat & Achache (1984) described the late Cretaceous and Cenozoic evolution of the Indian Ocean in much more detail, presenting rotations for the Central Indian Ridge (CIR) and Southeast Indian Ridge (SEIR) at 16 time steps in the Late Cretaceous and Cenozoic. With these closely spaced rotations they were able to show that the time of the major slowdown in spreading rate on the CIR, which is associated with the initial collision of India with Eurasia (Molnar & Tapponnier 1975), was around Chron 22, and the time of a major change in spreading direction on the CIR, associated with the hard collision of India with Eurasia, was around Chron 20.

SOUTHWEST INDIAN RIDGE

Spreading between Africa and Antarctica takes place along the SWIR between the Bouvet Triple Junction and the IOTJ. It is difficult to calculate Euler rotations for the SWIR due its history of very slow spreading rates and the complex pattern of spreading direction changes that dominated its development during the late Cretaceous and early Cenozoic. This left much of the ridge area dominated by very rough topography and difficult-to-interpret magnetic anomalies. The earliest models of spreading on the SWIR could not resolve the complex pattern of spreading direction changes and concluded that spreading could be quantified by a singe Euler pole for the entire late Cretaceous and Cenozoic period (e.g. Norton & Sclater 1979). However, Patriat *et al*. (1985) showed that there had been a major counter-clockwise (ccw) change in spreading direction in the late Cretaceous, starting around Chron 32, followed by a large clockwise (cw) change in spreading direction in the early Cenozoic, around Chron 24. The late Cretaceous ccw change in spreading direction generated a very complex pattern of topography along the western part of the SWIR as the large offset Bain transform fault went into extension and was replaced by a set of multiple short-offset ridge-transform segments (Royer *et al*. 1988; Sclater *et al*. 2005). The cw change in spreading direction around Chron 24 put the Bain transform under compression and the multiple offset ridge

segments were replaced by a long offset transform with the original geometry of the Bain transform.

The plate motion changes that caused this remarkable change in ridge configuration are difficult to resolve because of the slow spreading rates and the closely spaced fracture zones that dominate much of the ridge. Patriat (1987) only analysed data from east of the Bain transform and did not use fracture zone azimuths to constrain his rotations but rather used the alignment of the other two ridges at the IOTJ. Royer *et al*. (1988) used data from west of the Bain transform and incorporated satellite derived gravity data to map fracture zones. Molnar *et al*. (1988) were the first to assign quantitative errors to Euler rotations in the Indian Ocean, although they only directly calculated rotations for anomalies 20 and 33 on the SWIR. They determined rotations for other anomalies on the SWIR by summing rotations calculated for the CIR and SEIR. Nankivell (1997) used a three-plate method based on Shaw & Cande (1990) to solve for rotations on the SWIR and to quantitatively assign uncertainties, but he used the three plates of South America–Africa–Antarctica. The South America–Antarctica boundary of this three-plate circuit is very poorly constrained; along most of this ridge, which runs across the Weddell Sea, there are only data on the southern, Antarctic flank. To obtain a solution, Nankivell (1997) assumed that spreading was symmetrical on the South America–Antarctic Ridge. Bernard *et al*. (2005) used the method of Royer & Chang (1991) to determine rotations for anomalies 18, 23, 32, 33 and 34. They also determined a rotation for anomaly 28 although it was constrained solely by fitting fracture zones.

A complexity in using data from the SWIR is the presence of one or more late Cenozoic diffuse plate boundaries near the ridge axis within the African Plate. Several studies have proposed that fitting Euler rotations to magnetic anomalies along the SWIR requires that Africa be considered as two rigid plates, the Nubia Plate in the west and the Somalia Plate to the east (Chu & Gordon 1999; Lemaux *et al*. 2002; Royer *et al*. 2006), with a plate boundary that intercepts the SWIR near the Bain transform. More recently Horner-Johnson *et al*. (2007) showed that spreading rates along the SWIR axis are best fit by three plates, inserting the Lwandle Plate between the Nubia and Somalia plates. The largest amount of reported deformation along this boundary, about 25 km, is based on an observed misfit in anomaly 5 across the Bain transform reported by Royer *et al*. (2006). However, Patriat *et al*. (2008) showed that there were no apparent misfits for anomalies 6, 8 and 13 across the Bain transform and instead suggested that Royer *et al*. (2006) had misidentified the location of anomaly 5 on the African Plate west of the Bain transform. We also found that there are no large systematic misfits in the anomalies we analysed across the Bain transform. The effect of the Lwandle–Nubia and Nubia–Somalia rotations determined by Horner-Johnson *et al*. (2007) are relatively small; in Appendix A, we show that incorporating corrections for these rotations does not have a significant effect on our results. We did not use them in the analysis we present here.

CIR, SEIR AND CARLSBERG RIDGE

Spreading between India and Africa runs from the Gulf of Aden to the IOTJ along the Carlsberg Ridge and CIR. Current spreading rates along this plate boundary varies from very slow on the Carlsberg Ridge to moderately slow on the CIR near the triple junction. However, in the late Cretaceous and early Cenozoic, prior to the large decrease in spreading rate around Chron 22, spreading rates along this boundary were very fast and the anomalies formed at that time are relatively straightforward to identify. Spreading between Antarctica and India (Australia) currently occurs along the SEIR from the IOTJ east to the Macquarie triple junction. However prior to the change in India Plate motion at roughly Chron 20, India and Australia were two plates separated by a spreading ridge that passed through the Wharton Basin and north of Australia (McKenzie & Sclater 1971; Liu *et al*. 1983). The early Cenozoic spreading between India, Africa and Antarctica on the CIR and SEIR was mapped in detail by Patriat (1987). Additional constraints on CIR and SEIR spreading in the early Cenozoic and particularly on the location of the L'Astrolabe and La Boussole fracture zones and the trace of the IOTJ on the Indian Plate were given by Dyment (1993). A survey of the African flank of the CIR southeast of Reunion mapped the change in spreading direction around Chron 20 as recorded in the topography and magnetic field (Dyment *et al.* 1999).

There are several problems in analysing rotations between India and Africa. The first problem is that there has been considerable deformation within the Indian Plate over the last 20 Ma across a broad diffuse plate boundary that runs from the CIR near 5°S to the Java–Sumatra Trench near 100°E (Wiens *et al*. 1985; DeMets *et al*. 1988). The portion of the Indian Plate south of this region of deformation was originally considered to form a distinct, separate Australian Plate. An additional diffuse plate boundary, active within the last 8 Ma or so, was later identified within the Australian Plate near the 90°E ridge (Royer & Gordon 1997). The portion of the Australian Plate west of that deformation zone was identified as a distinct rigid plate and referred to as the Capricorn Plate. Fortunately, the motion between the Indian Plate and the Capricorn Plate is well constrained by detailed magnetic studies along the Carlsberg and CIRs (DeMets *et al*. 2005) and corrections can be made for this motion when combining data from the Indian side of the Carlsberg Ridge with data from the Capricorn side of the CIR. The diffuse plate boundary between the Capricorn and Australian plates is more poorly constrained and we only use data on the SEIR from west of the 90°E ridge in our calculation of SEIR rotations for anomalies 13o and 18o. In this paper we calculate rotations between the Somalia, Antarctic and Capricorn plates.

We note that the early studies of McKenzie & Sclater (1971) and Norton & Sclater (1979) combined data from the Carlsberg Ridge with data from the CIR without a correction for India–Capricorn motion, which was unknown at the time. Molnar *et al*. (1988) also combined these data sets without a correction, but noted that there may be a problem related to the motion between the Indian and Capricorn plates which was just being recognized when they wrote their paper. Patriat (1987) and Patriat & Achache (1984) avoided this issue because they did not use data from the Carlsberg Ridge to constrain motion between the African and Indian (Capricorn) plates.

A second and more difficult problem is that prior to the large cw change in spreading direction between Africa and India around Chron 20, spreading on the Carlsberg Ridge was offset by a very long transform, the Chagos/Mauritius FZ, from spreading on the CIR. An unresolved issue is whether spreading on these two ridges, as it was occurring, was part of the same two-plate system (India–Africa) or whether some of the motion on the Carlsberg Ridge was taken up on another boundary. This question is pertinent because spreading between Africa and India in the late Cretaceous originally started in the Mascarene Basin around anomaly 34 (Schlich 1982; Masson 1984). Rifting between India and the Seychelles Bank started around Chron 29 (Norton & Sclater 1979) but spreading in the Mascarene basin did not cease until roughly

Table 1. Ages of magnetic anomalies.

Anom ID	Age (Ma)
13o	33.738
18o	39.464
20y	41.590
20o	42.774
21y	45.346
21o	47.235
22o	49.427
23o	51.901
24o	53.808
25y	56.665
26y	58.379
27y	61.650
28y	63.104
29o	65.118

Note: Gradstein *et al*. (2004).

Chron 27 (Dyment 1991). Thus, for several million years spreading was occurring both in the Mascarene basin and on the Carlsberg Ridge simultaneously and during this time there would have been a distinct Seychelles microplate that developed between the two active ridges (Masson 1984; Dyment 1991; Plummer 1996; Todal & Eldholm 1998; Royer *et al*. 2002). The time of the initiation and cessation of motion of this microplate is not known. Another unresolved issue is the role of the Amirante Trench along the south side of the Seychelles Bank. Originally this feature was thought to have been the locus of subduction in the late Cretaceous and earliest Cenozoic (Fisher *et al*. 1968; Masson 1984; Mart 1988; Dyment 1991; Plummer 1996) based, in large part, on a single K-Ar date of 82 Ma on a dredged basalt collected in the 1960s. However, Stephens *et al*. (2009) recently analysed a fresh gabbro from a dredge collected in the 1990s (Tararin & Lelikov 2000) and obtained a much younger Ar-Ar date of 52 Ma, throwing into question the age and origin of the feature. In addition, there may also have been spreading, which continued until as late as Chron 24 in the Gop Basin, on the north side of the Carlsberg Ridge (Yatheesh *et al*. 2009). In this paper we will show that, in addition to the well-documented motion between the Indian and Capricorn plates since 20 Ma, spreading on the Carlsberg Ridge does not follow the same Euler rotations as the rest of the CIR prior to Chron 22.

A final problem is that the pattern of magnetic anomalies and fracture zones that developed on the Carlsberg Ridge in the early Cenozoic is very complex. The magnetic anomaly pattern is severely disrupted by several propagating ridges that were active in this period (Dyment 1998; Chaubey *et al*. 2002) and there is a lack of well-mapped fracture zones. As a consequence it is difficult

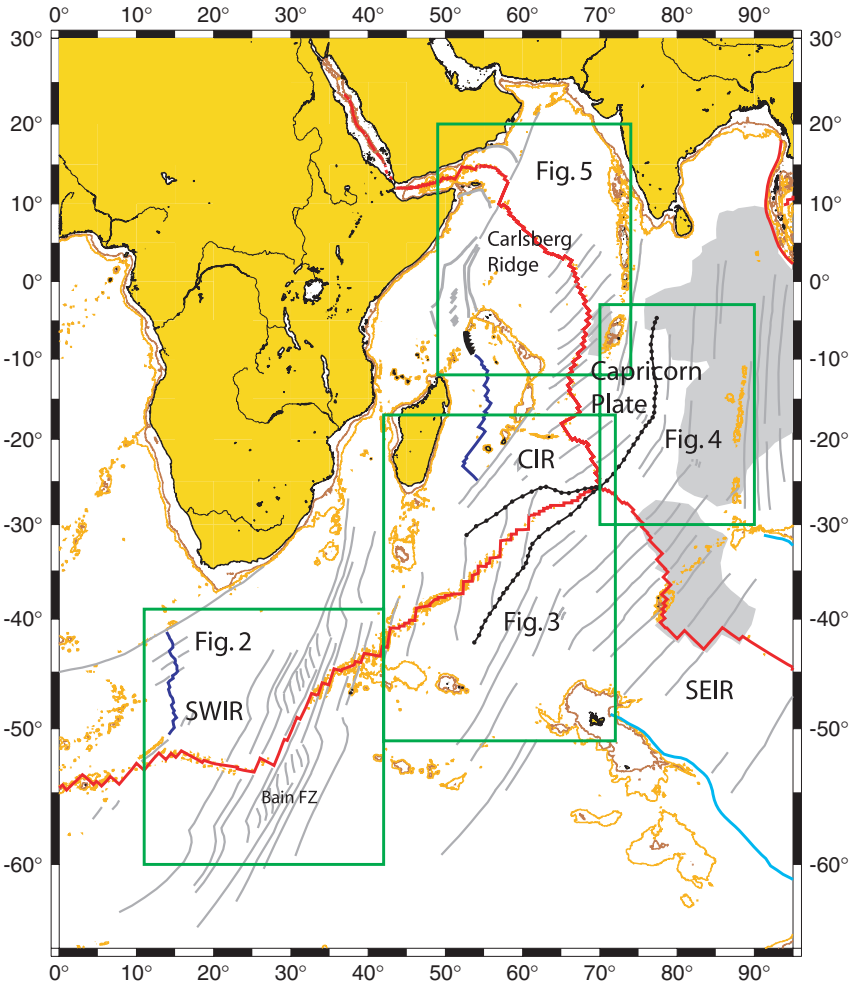

Figure 1. Tectonic elements in the Indian Ocean. Active spreading ridges are shown in red. Black chains mark triple junction traces. Grey shaded areas demarcate regions of diffuse plate boundaries between the Indian, Capricorn and Australian plates since roughly 8 Ma.

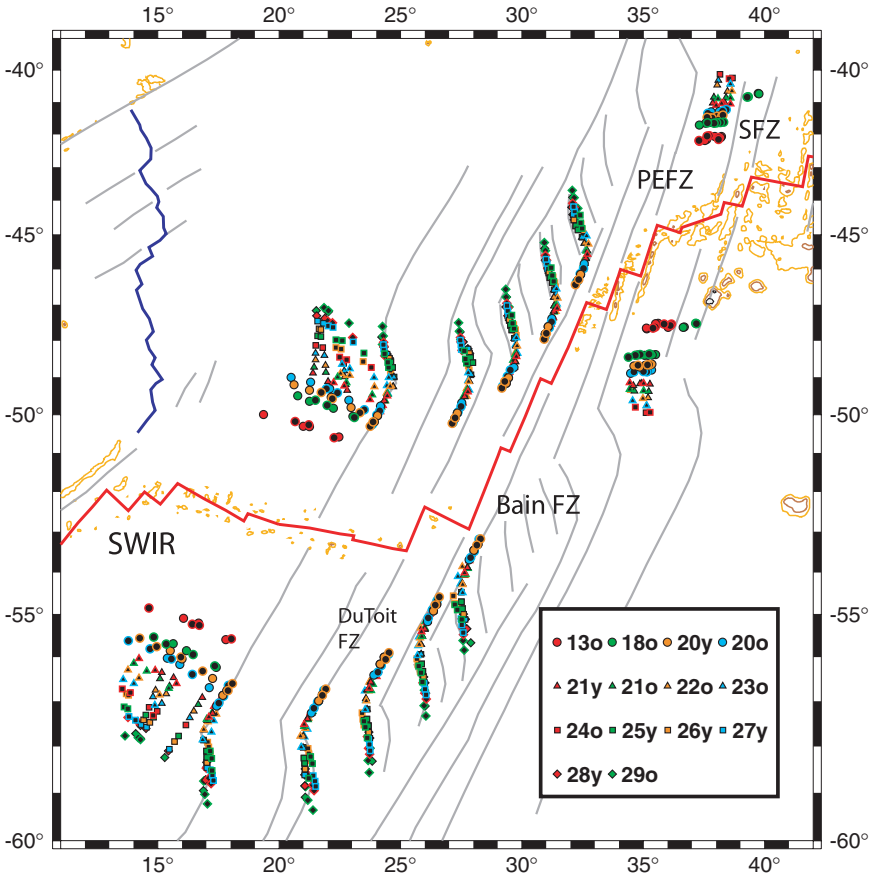

Figure 2. Magnetic anomaly picks and fracture zone locations used in this study from the western end of the SWIR. PEFZ = Prince Edward FZ, SFZ = Simpson FZ. Fixed points are shown with black rims and coloured cores, rotated points (rotation set 2) by coloured rims and black cores.

to reconstruct the original ridge geometry when fitting magnetic anomalies from the two ridge flanks (Royer *et al*. 2002). In particular Royer *et al*. (2002) noted that there is an along-isochron 'sliding problem' when positioning India relative to Africa. They proposed a series of fits for anomalies 20 to 26 on the Carlsberg Ridge that moved Africa about 60 kms west relative to India compared to the earlier fit of Molnar *et al*. (1988). Our reconstructions suggest that the position of Africa was closer to the original position proposed by Molnar *et al*. (1988).

THIS STUDY

In this study we calculated three-plate solutions for anomalies 13o, 18o, 20y, 20o, 21y, 21o, 22o, 23o, 24o, 25y, 26y, 27y, 28y and 29o (See Table 1 for ages). Because of the problems discussed above concerning (1) identifying and dating fracture zone segments on the SWIR and (2) incorporating data from the Carlsberg Ridge with the CIR, we calculated four sets of rotations. The first set of rotations (Set 1: 'Basic') used data from the CIR, SEIR and SWIR but without any fracture zone constraints from the SWIR or data from the Carlsberg Ridge. For the second set of rotations (Set 2: 'With SWIR FZs') we used synthetic flowlines based on the first set of rotations to assign ages to portions of fracture zones on the SWIR near the Bain fracture zone and then calculated a set of rotations in which SWIR fracture zones were added to the 'Basic' data set. The third set of rotations (Set 3: 'With Carlsberg') added magnetics data from the Carlsberg Ridge to the 'Basic' data set. Finally we calculated a fourth set of rotations (Set 4: 'All') in which data from the Carlsberg Ridge and the SWIR fracture zones were added to the 'Basic' data set.

DATA

The magnetic anomaly and fracture zone data used to constrain the rotations are shown in Figs 1–5. The magnetic anomaly data set was constructed mainly from a data compilation put together in the early 1990s under the aegis of the Indian Ocean Data Compilation Project (IODCP, Sclater *et al*. 1997). Additional data were taken from sources that were not included in the IODCP including surveys of the Carlsberg Ridge (Chaubey *et al*. 2002; Royer *et al*. 2002), a survey of the African flank of the CIR southeast of Mauritius near the location of the Chron 20 change in spreading direction (Dyment *et al.* 1999) and many transits across the SWIR (Patriat *et al*. 2008). The magnetic anomaly picks in the IODCP compilation were vetted by us and occasionally modified. For example, magnetic anomaly picks on the SWIR west of the Bain fracture zone were modified to better conform to the original picks in the work of Royer *et al*. (1988). Constraints for the L'Astrolabe and La Boussole fracture zones on the Indian Plate were taken primarily from Dyment (1993). Data from the northern flank of the Carlsberg Ridge (Fig. 5), located on the Indian Plate, were rotated back to their positions relative to the Capricorn plate using the 20 Ma (anomaly 6no) India–Capricorn rotation of DeMets *et al*. (2005). This rotation (Lat. = 3.08°S, Long. = 75.79°E, Angle = 3.22°) is well constrained and the uncertainty ellipses on the rotated points are small (Fig. 5, inset).

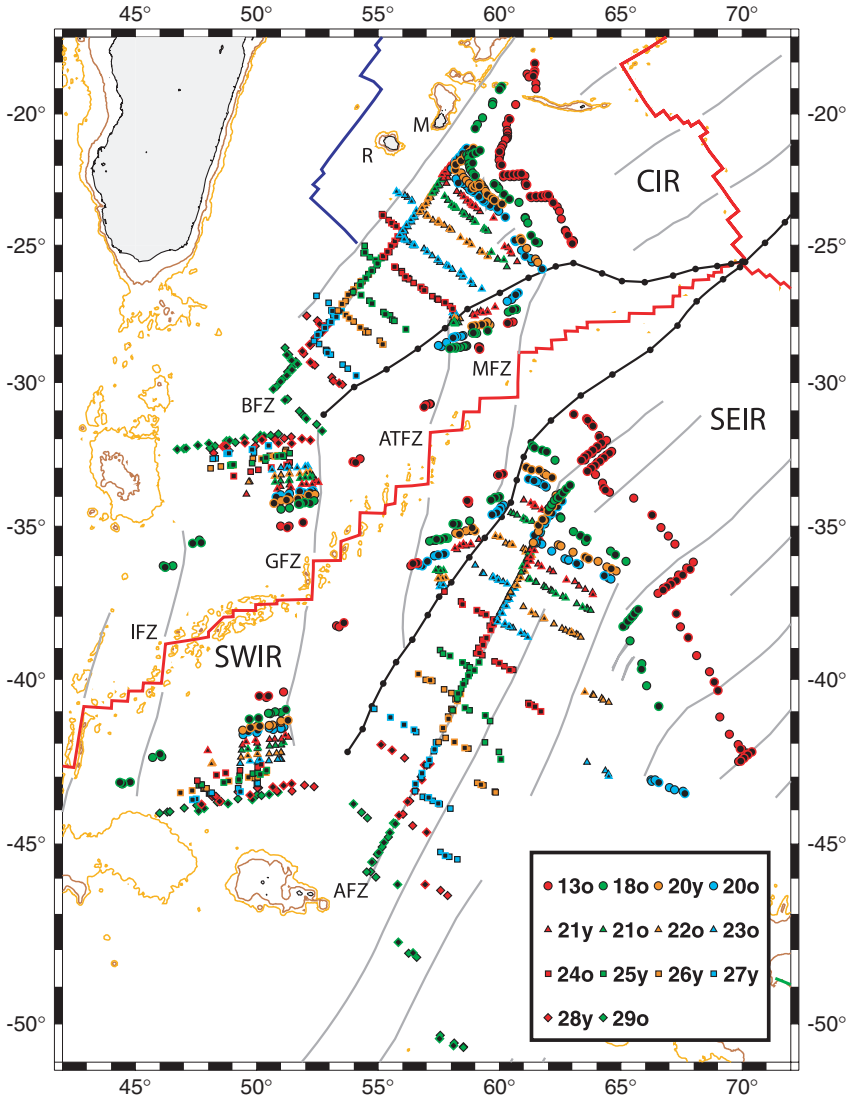

Figure 3. Magnetic anomaly picks and fracture zone locations used in this study from the eastern end of the SWIR and from the African side of the CIR and Antarctic side of the SEIR. IFZ = Indomed FZ, GFZ = Gallieni FZ, ATFZ = Atlantis FZ, MFZ = Melville FZ, R = Reunion, M = Mauritius, AFZ = L'Astrolabe FZ, BFZ = La Boussole FZ.

For data set 1 ('Basic'), rotations were calculated for anomalies 13o to 29o. For data set 2 ('With SWIR FZs') rotations were calculated for anomalies 20y to 29o. For data sets 3 and 4 ('With Carlsberg' and 'All'), which incorporated Carlsberg Ridge data, rotations were only calculated for anomalies 20y to 26y since prior to anomaly 26y the spreading between India and Africa was taken up in whole or in part in the Mascarene basin.

After the calculation of the first set of rotations ('Basic'), synthetic flowlines along the SWIR were calculated using the new rotations (Fig. 6a). It was observed that although these synthetic flowlines captured the basic change in spreading direction on the SWIR, in detail the flowlines were not very smooth. It was also apparent that constraints from the Bain fracture zone splays would smooth out the fluctuations in the synthetic flowlines. Consequently, the synthetic flowlines were used to assign ages to three splays of the Bain fracture zone and two fracture zones, the DuToit and an unnamed one, 150 and 500 km west of the Bain fracture zone, respectively. These five fracture zone splays were then digitized (Fig. 7) and roughly 60 km long sections were included in the constraints for each rotation in the second set of rotations ('With SWIR FZs'). As we will discuss later, trajectories based on rotations using the SWIR fracture zone constraints are much smoother (Fig. 6b).

METHOD

We followed the method of Hellinger (1981) and determined reconstruction parameters by dividing the data into multiple segments and fitting great circles to the reconstructed data in each segment. The magnetic anomalies and fracture zones were used to define up to 25 segments. We used the best-fitting criteria and statistical techniques of Chang (1987, 1988), Royer & Chang (1991) and Kirkwood *et al*. (1999) to calculate rotation parameters and estimate uncertainty ellipses. This method requires that an estimate of the error in the position be assigned to every data point. Although it is possible to assign a separate error estimate to each data point, varying it, for example, for the type of navigation, this level of detail was beyond the scope of this study. Instead, based on our experience with other data sets, we generally assigned an estimate of 3.5 km for all magnetic

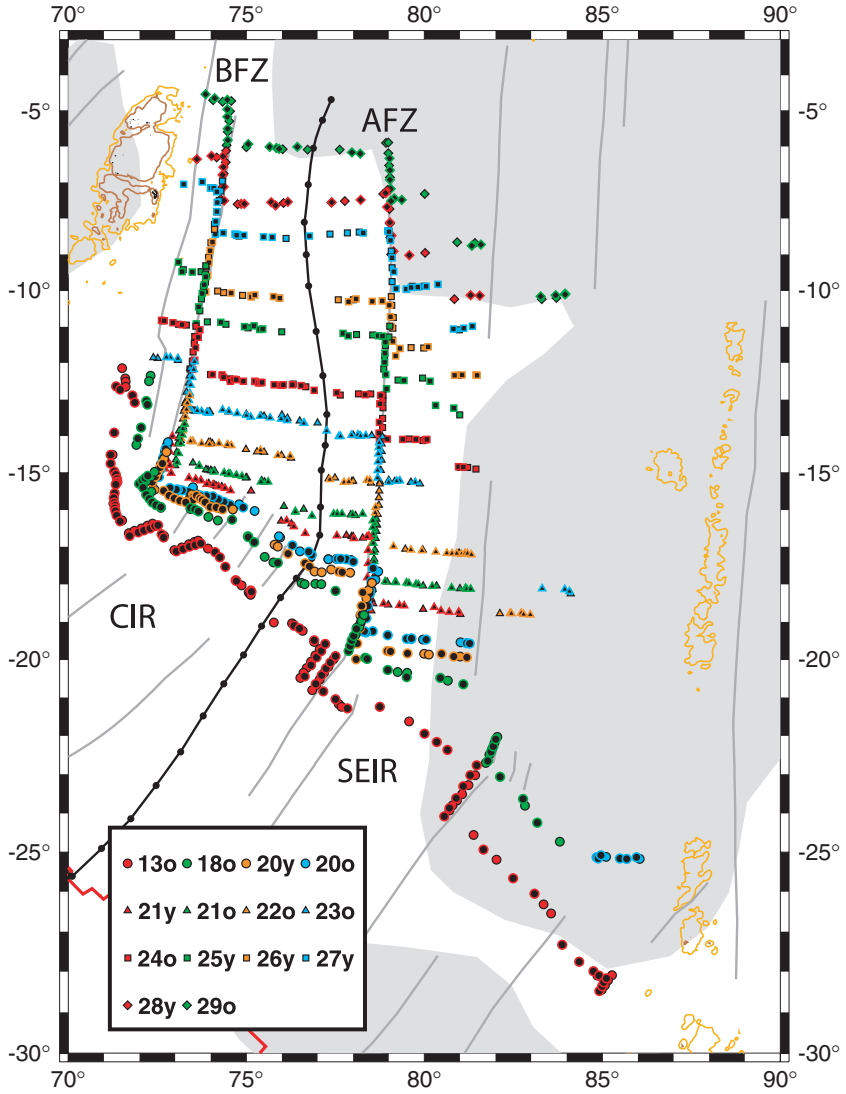

Figure 4. Magnetic anomaly picks and fracture zone locations used in this study from the Capricorn side of the CIR and SEIR. AFZ = L'Astrolabe FZ, BFZ = La Boussole FZ.

anomaly points and 5 km for all fracture zone crossings. One major exception to this rule was that we assigned an error estimate of 5 km to anomaly points older than anomaly 24o on the SWIR west of the Bain fracture zone where data coverage is particularly sparse and anomaly identifications are difficult due to the slow spreading rates. In places where we applied corrections for intraplate deformation (e.g. India–Capricorn) we assigned an error estimate of 6 km to the anomaly points.

The quantitative method we used for fitting tectonic constraints requires that a minimum of three data points are present along any segment that is going to be included in the solution (two on one flank of the ridge and one on the conjugate side). Hence only picks, which met this requirement were used. We also tended to be very cautious in including picks along the SWIR since anomaly identifications are often problematical. In fact, one advantage of calculating a three-plate solution is that fewer data are needed from any one-plate boundary and, consequently, one can be more conservative in the choice of magnetic anomaly picks.

As part of the solution using the Chang (1987, 1988) method a statistical parameter, $\hat{\kappa}$, is returned which is an evaluation of the accuracy of the assigned errors in the location of the data points. If $\hat{\kappa}$ is near 1, the errors have been correctly assigned; if $\hat{\kappa}$ is $\gg 1$ the errors are overestimated; and if $\hat{\kappa}$ is $\ll 1$ the errors are underestimated. For most of our data sets, the value of $\hat{\kappa}$ was near 1, indicating that the error estimates were reasonable. For Chrons where $\hat{\kappa}$ was greater than 1, the error values were overestimated by the $\sqrt{\hat{\kappa}}$, and for Chrons where $\hat{\kappa}$ was less than 1, errors were underestimated by the $\sqrt{\hat{\kappa}}$. Although a $\hat{\kappa}$ of 1.0 could be obtained by dividing the original error estimates by $\sqrt{\hat{\kappa}}$, this rescaling makes no difference in the location of the poles and only a minor difference in the size of the uncertainty ellipses for all of these rotations. Consequently, for the sake of consistency, we cite the results using the original error estimates.

RESULTS

Rotations and covariance matrices for the four sets of data constraints are presented in Tables 2–5. The rotation poles and their uncertainty ellipses are show in Figs 8–10 for the CIR, SEIR and

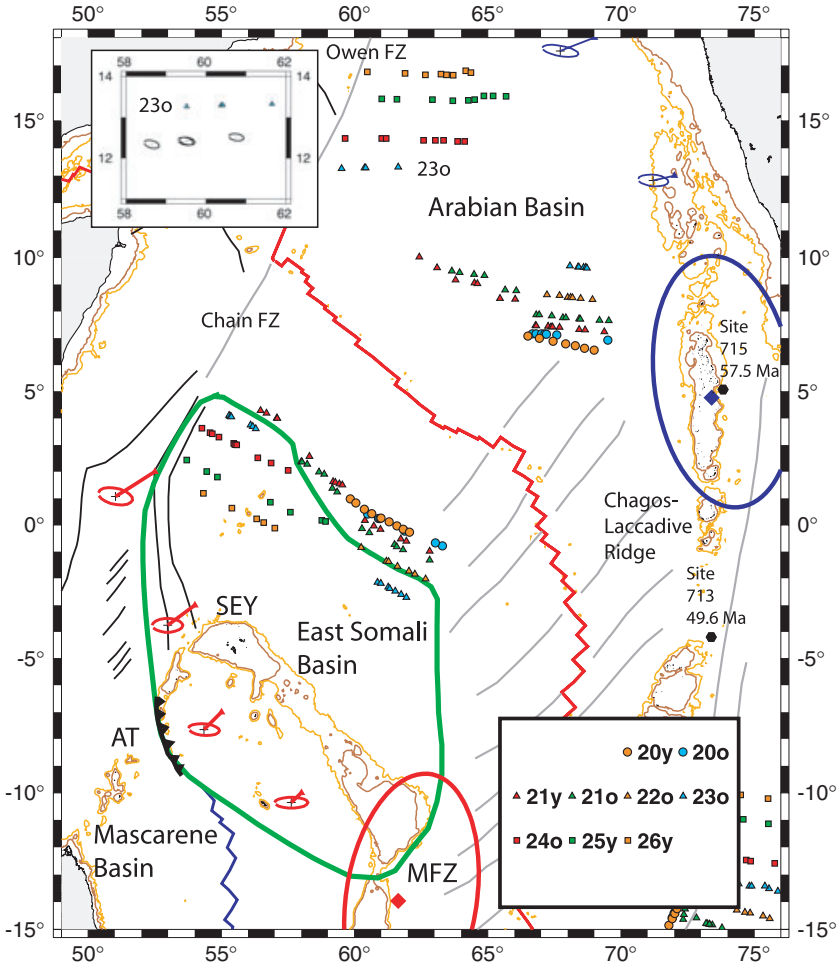

Figure 5. Magnetic anomaly picks used in this study from the Carlsberg Ridge. Inset shows an example (with uncertainty ellipses) of rotating anomalies on north (Indian Plate) side of the Carlsberg Ridge back to the Capricorn Plate by the anomaly 6no Ind–Cap rotation of DeMets *et al*. (2005). AT = Amirante Trench, SEY = Seychelles. Heavy green line outlines extent of Seychelles microplate. See caption of Fig. 20 for explanation of red and blue ellipses and red and blue diamonds.

SWIR, respectively. As a demonstration of the accuracy of the rotations, Figs 2–4 also show the data picks from the CIR, SEIR and SWIR rotated to their conjugate locations using the 'With SWIR FZs' rotations constrained with data set 2.

For all three ridges (CIR, SEIR and SWIR) the rotations constrained by data set 1 ('Basic') have the largest error ellipses and produce pole paths that zigzag back and forth around the other pole paths. Adding constraints from the SWIR fracture zones (data set 2) reduces this zigzagging substantially for all three ridges, and adding the Carlsberg Ridge constraints (data sets 3 and 4) leads to a very smooth pole path for the CIR and SEIR. An unexpected result is that the two sets of rotations constrained with data from the Carlsberg Ridge (sets 3 and 4) diverge from the two sets of rotations that do not include Carlsberg Ridge constraints (sets 1 and 2) prior to anomaly 22o. We discuss the implications of this finding at length in a later section.

In Figs 8–10 the rotation poles from previous classical two-plate reconstructions are shown for comparison. The agreement between the Patriat (1987) rotations and our new rotations constrained with data sets 1 and 2 is often good although the anomalies for which there is good agreement are not the same on the CIR and SEIR highlighting the difficulty in obtaining a perfect three-plate closure as noted by Patriat & Segoufin (1988). An unexpected result of this comparison is that the zigzag pole path of Patriat (1987), from reconstructions constrained by a minimum number of fracture zones, is more like our results than the almost straight path of Royer & Sandwell (1989) and Royer *et al*. (1988), which were based on reconstructions made with strong constraints from fracture zones based on detailed satellite mapping. Zigzaging paths could be a reflection of the necessary motion adjustments of each plate with respect to the other two. The three-plate reconstruction is clearly a powerful method to tackle these difficulties.

TRAJECTORIES AND SPREADING RATES

An instructive way to look at the motion predicted by the new rotations is to plot trajectories and spreading rates at several points along the plate boundary. To calculate the spreading rates we used ages from the geomagnetic polarity timescale of Gradstein *et al*. (2004) (GOS04). We used GOS04 rather than Cande & Kent (1995) (CK95) because GOS04 gave a smoother spreading rate history around Chrons 24 and 18 and therefore is probably more accurate in this time interval. We illustrate the difference in Fig. 11 in which we compare spreading rates on the SEIR based on rotation set 2 for

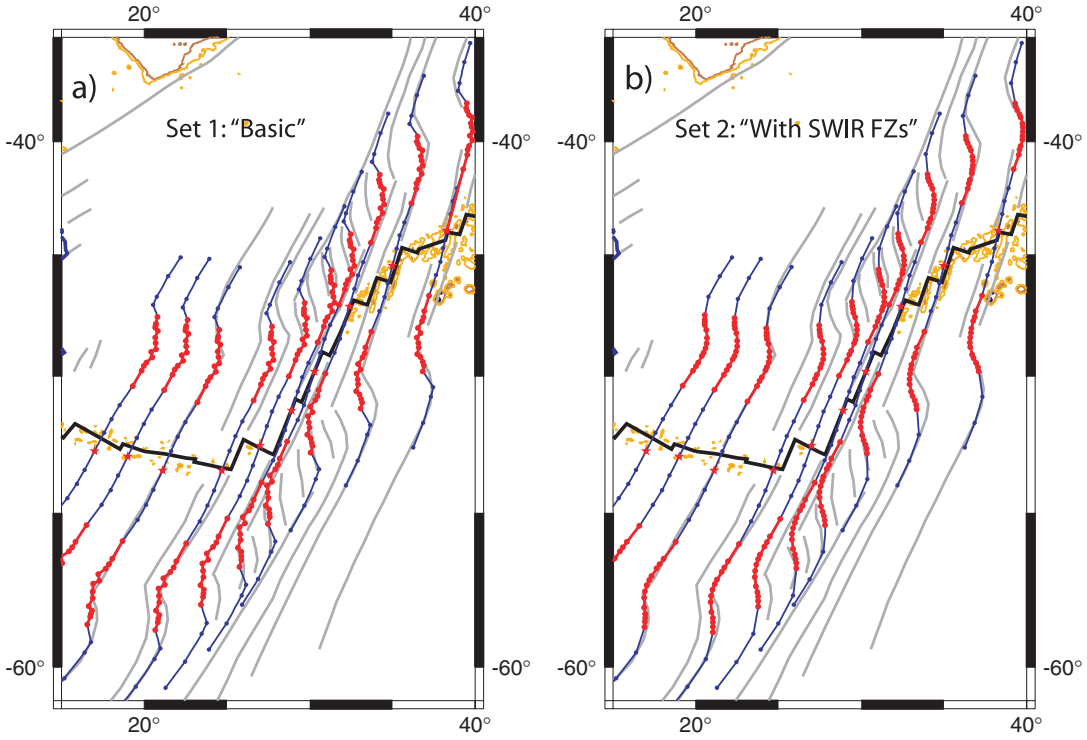

Figure 6. (a) Synthetic flowlines near the Bain FZ for the motion between the Antarctica and Somalia plates based on rotation set 1 ('Basic'). (b) Synthetic flowlines for the same motion based on rotation set 2 ('With SWIR FZs') which incorporates fracture zone constraints based on satellite gravity imagery near the Bain FZ. Note that the flowlines incorporating the SWIR FZ constraints (b) are much smoother than the 'Basic' flowlines (a).

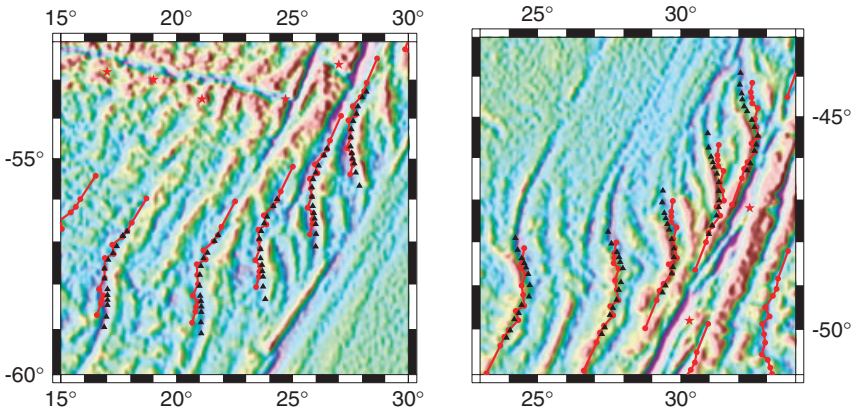

Figure 7. Satellite gravity imagery over the southern (left-hand panel) and northern (right-hand panel) splays of the Bain FZ with synthetic flowlines based on rotation set 1 ('Basic') shown in red. The black triangles show the fracture zone points that were digitized based on the gravity and synthetic flowlines.

the two timescales. This difference reflects the use of a different set of calibration points in the early Cenozoic by GOS04, and especially by the age adjustment of a long contentious calibration point within Chron C21n (Gradstein *et al*. 2004).

CIR AND SEIR TRAJECTORIES AND SPREADING RATES

The predicted motion of three points on the Capricorn Plate since anomaly 29o, two relative to the Somalia Plate (Cap–Som) and one relative to the Antarctic Plate (Cap–Ant), is shown in Fig. 12. For clarity we only show the trajectories for two of the four rotation sets ('With SWIR FZs' and 'With Carlsberg'; sets 2 and 3) and omitted uncertainty ellipses. In Figs 13a and b we zoom in on one of the Cap–Som trajectories and the Cap–Ant trajectory, respectively, and show the trajectories for all four rotation sets with their 95 per cent confidence zones between anomalies 24o and 13o. These figures confirm that the 'Basic' rotations (data set 1) are not well constrained, with large uncertainty ellipses, and predict trajectories that zigzag around. The trajectories constrained by the 'With SWIR FZs' rotations (data set 2) are considerably smoother than the 'Basic' trajectories but still have relatively large 95 per cent confidence zones and moderate zigzags between anomalies 22o and 20y. The two rotation sets constrained by the Carlsberg magnetic anomaly picks, data sets 3 and 4, give the smoothest paths for anomalies 22o to 20y, although they deviate from the 'Basic' and 'With SWIR FZs' trajectories prior to anomaly 22o. A distinct kink in both the

Table 2. Finite rotations for data set 1 ('Basic').

Anom	Lat. (°N)	Long. (°E)	Angle (°)	$\hat{\kappa}$	a	b	c	d	e	f	points	segs
						Capricorn–Antarctica						
13o	−16.58	−149.67	19.89	0.59	2.90	12.58	67.56	−5.50	−29.19	13.24	171	22
18o	−16.77	−149.92	23.52	0.63	7.98	40.28	230.89	−16.29	−93.21	39.07	125	19
20y	−16.25	−150.67	24.73	0.77	21.68	105.04	530.16	−37.63	−191.16	70.81	97	12
20o	−16.84	−151.94	25.20	0.62	3.86	19.91	123.80	−6.85	−42.97	16.66	119	12
21y	−16.26	−153.36	26.52	0.49	27.60	136.54	691.87	−46.78	−236.83	83.32	93	10
21o	−13.72	−152.06	28.46	1.57	16.18	82.98	439.33	−26.50	−140.30	46.26	128	10
22o	−15.46	−156.39	29.24	1.33	15.89	77.81	394.52	−24.55	−124.62	42.04	101	10
23o	−13.04	−156.28	32.36	0.75	8.77	42.45	220.16	−11.91	−61.85	19.06	106	11
24o	−12.90	−158.25	34.46	0.86	15.64	77.61	406.78	−19.55	−102.35	27.72	86	10
25y	−12.98	−161.45	37.21	0.57	44.15	220.62	1132.42	−49.24	−252.76	59.04	62	9
26y	−12.23	−161.74	39.40	2.21	55.66	290.94	1554.38	−58.42	−312.42	65.03	63	8
27y	−9.54	−161.02	43.85	1.18	46.48	236.97	1231.39	−38.34	−200.13	34.74	66	9
28y	−8.81	−161.38	45.81	0.57	141.76	655.23	3078.79	−98.34	−463.72	71.95	61	9
29o	−9.71	−164.50	48.36	0.62	14.16	81.56	508.00	−10.44	−66.86	10.92	71	11
						Capricorn–Somali						
13o	–16.32	–132.31	18.93	0.59	8.90	26.64	87.88	−8.66	−27.97	9.62	171	22
18o	−16.76	−131.58	22.22	0.63	21.05	72.02	259.74	−20.47	−72.94	21.42	125	19
20y	−17.13	−132.08	23.18	0.77	49.13	172.73	617.48	−50.41	−180.42	53.88	97	12
20o	−17.91	−132.80	23.40	0.62	12.71	44.64	163.45	−13.16	−46.88	15.13	119	12
21y	−17.93	−133.84	24.22	0.49	61.19	222.78	822.32	−62.09	−228.22	64.87	93	10
21o	−15.97	−133.40	26.39	1.57	40.08	148.83	558.20	−39.33	−146.65	40.08	128	10
22o	−18.47	−137.57	26.15	1.33	36.62	134.93	505.44	−33.21	−124.00	32.18	101	10
23o	−15.98	−138.71	29.37	0.75	22.73	81.85	299.60	−18.83	−68.70	17.36	106	11
24o	−15.77	−141.17	31.31	0.86	40.53	147.10	541.31	−31.11	−113.86	25.85	86	10
25y	−16.90	−145.42	33.18	0.57	124.42	447.25	1621.57	−81.09	−293.13	55.23	62	9
26y	−15.99	−146.13	35.57	2.21	163.85	613.64	2318.62	−103.26	−390.39	67.91	63	8
27y	−14.52	−147.32	39.57	1.18	163.01	595.61	2200.65	−84.96	−313.89	47.16	66	9
28y	−14.42	−148.26	41.20	0.57	302.76	1143.36	4343.88	−140.62	−535.34	68.13	61	9
29o	−15.83	−152.43	42.73	0.62	78.13	295.89	1140.56	−26.85	−103.32	11.18	71	11
						Antarctica–Somalia						
13o	12.69	–44.61	5.67	0.59	5.71	5.12	5.63	−2.35	−2.53	3.99	171	22
18o	13.80	−43.75	7.05	0.63	6.60	5.69	5.56	−0.01	−0.79	6.80	125	19
20y	11.85	−42.54	7.53	0.77	10.35	8.71	8.15	−0.99	−1.65	6.52	97	12
20o	11.95	−42.32	7.87	0.62	7.44	6.65	6.87	−3.38	−3.81	5.45	119	12
21y	11.37	−40.75	8.50	0.49	13.23	12.55	13.05	−3.60	−4.47	8.58	93	10
21o	9.44	−41.35	8.82	1.57	12.35	12.55	13.51	−6.22	−6.98	9.01	128	10
22o	9.32	−39.61	9.22	1.33	14.02	16.29	20.70	−9.63	−11.89	14.99	101	10
23o	9.45	−41.34	9.62	0.75	12.57	13.67	16.53	−9.88	−11.48	13.07	106	11
24o	10.39	−43.41	9.97	0.86	18.93	17.89	18.62	−13.95	−13.96	17.33	86	10
25y	8.53	−42.37	10.42	0.57	73.61	78.79	88.26	−68.40	−79.09	84.07	62	9
26y	9.16	−44.74	10.69	2.21	85.13	86.67	91.03	−74.60	−80.91	83.78	63	8
27y	4.84	−41.98	11.00	1.18	128.65	137.90	152.25	−138.39	−153.45	165.95	66	9
28y	2.79	−41.12	11.33	0.57	138.37	154.91	177.56	−148.23	−171.32	180.58	61	9
29o	1.82	−39.51	11.68	0.62	108.85	119.72	134.05	−132.27	−149.26	177.19	71	11

Notes: a, b, c, d, e and f are covariances and have units of 10^{-7} radians^2.
Covariance matrices are reconstructed from the equation

$$1/\hat{\kappa} * \begin{pmatrix} a & b & c \\ b & d & e \\ c & e & f \end{pmatrix}.$$

Cap–Som and Cap–Ant trajectories is observed in all four rotation sets at anomaly 20o; a straight line can be drawn through the 95 per cent confidence zones for all trajectories between anomalies 22o and 20o.

Spreading rates for the same representative points for the CIR and SEIR based on the 'With SWIR FZs' rotation set are shown in the insets in Figs 13a and b, respectively. Error bars for the spreading rates were estimated by calculating stage poles for each interval and using the covariance matrices of the stage poles to plot a 95 per cent confidence ellipse for each step in the trajectory. The uncertainty in spreading rates on the CIR and SEIR varied between 4 and 8 per cent.

The spreading rate history shows that both the CIR and SEIR underwent long continuous slowdowns starting around Chron 23o (51.9 Ma) and ending around Chron 21y (45.3 Ma), an interval of 6.6 Ma, during which time the spreading rates dropped from 120 to 40 mm yr^{-1} on the CIR and from 140 to 60 mm yr^{-1} on the SEIR. The change in azimuth around Chron 20 was abrupt on both ridges

Table 3. Finite rotations for data set 2 ('With SWIR FZs').

Anom	Lat. (°N)	Long. (°E)	Angle (°)	$\hat{\kappa}$	a	b	c	d	e	f	Points	Segs
						Antarctica–Africa						
20y	−16.46	−150.87	24.66	0.87	12.28	53.17	244.10	−18.26	−84.35	30.92	117	17
20o	−16.90	−152.00	25.18	0.74	3.19	14.21	74.94	−4.69	−24.41	9.60	149	17
21y	−15.36	−152.45	26.82	0.61	12.57	56.36	263.86	−18.44	−85.66	29.89	123	15
21o	−14.51	−152.87	28.16	1.73	10.32	46.28	217.80	−14.52	−68.03	22.77	132	15
22o	−14.66	−155.55	29.51	1.31	9.73	43.79	206.51	−12.97	−60.84	20.41	131	15
23o	−12.78	−155.99	32.47	0.74	6.52	28.36	132.07	−7.71	−35.72	11.25	136	16
24o	−12.73	−158.06	34.53	0.72	9.70	41.70	189.82	−10.26	−46.25	13.21	116	15
25y	−12.37	−160.66	37.50	0.52	20.85	92.57	428.19	−20.43	−94.53	23.42	92	14
26y	−11.75	−161.08	39.65	1.35	22.80	105.13	504.15	−20.64	−99.13	21.60	93	13
27y	−9.05	−160.34	44.17	1.15	23.24	109.05	528.21	−17.17	−83.89	15.42	96	14
28y	−7.86	−160.12	46.47	0.66	76.35	321.51	1379.98	−46.67	−201.04	31.28	91	14
29o	−8.49	−162.87	49.05	0.53	9.94	47.89	251.76	−5.27	−28.70	5.29	101	16
						Capricorn–Somalia						
20y	−17.37	−132.21	23.06	0.87	16.90	62.34	239.28	−18.75	−71.96	22.77	117	17
20o	−18.00	−132.85	23.35	0.74	4.71	17.28	69.90	−5.30	−20.03	7.42	149	17
21y	−16.91	−133.23	24.76	0.61	15.03	58.57	237.96	−16.68	−66.66	20.19	123	15
21o	−16.80	−133.97	25.87	1.73	11.93	46.73	189.65	−12.62	−50.14	14.98	132	15
22o	−17.50	−136.87	26.72	1.31	11.32	44.31	180.75	−11.53	−46.36	13.58	131	15
23o	−15.72	−138.50	29.55	0.74	7.87	29.64	116.21	−7.36	−28.45	8.46	136	16
24o	−15.65	−141.06	31.40	0.72	11.21	42.98	171.51	−9.77	−38.09	10.31	116	15
25y	−15.71	−144.32	34.05	0.52	20.97	81.26	326.69	−15.25	−60.36	13.33	92	14
26y	−14.95	−145.15	36.37	1.35	28.01	114.16	482.05	−20.22	−85.15	17.06	93	13
27y	−13.35	−146.15	40.64	1.15	29.80	120.69	507.60	−17.76	−74.40	13.15	96	14
28y	−12.86	−146.60	42.71	0.66	74.98	299.52	1216.41	−39.09	−159.15	22.81	91	14
29o	−13.72	−149.94	44.76	0.53	11.50	48.85	223.55	−4.85	−21.65	3.81	101	16
						Antarctica–Somalia						
20y	11.86	−42.30	7.53	0.87	2.50	1.95	2.32	−2.05	−2.57	6.33	117	17
20o	11.91	−42.15	7.87	0.74	1.66	1.23	1.79	−1.92	−2.45	5.09	149	17
21y	11.27	−41.55	8.48	0.61	1.92	1.59	2.31	−2.71	−3.50	7.72	123	15
21o	9.73	−40.67	8.82	1.73	2.27	1.99	2.78	−3.73	−4.33	9.35	132	15
22o	9.25	−40.65	9.21	1.31	2.73	2.54	3.75	−4.71	−5.55	11.23	131	15
23o	9.31	−41.53	9.61	0.74	2.78	2.77	4.22	−4.41	−5.38	9.45	136	16
24o	10.16	−43.30	9.96	0.72	4.74	4.34	5.65	−7.41	−7.62	13.98	116	15
25y	9.86	−45.24	10.49	0.52	11.49	13.75	19.32	−20.16	−26.01	39.54	92	14
26y	10.64	−47.47	10.78	1.35	12.67	14.09	17.47	−18.85	−22.53	33.30	93	13
27y	7.10	−45.80	11.08	1.15	16.23	17.51	21.93	−24.59	−28.43	42.88	96	14
28y	4.75	−44.79	11.39	0.66	13.59	15.49	20.54	−23.54	−28.38	44.86	91	14
29o	4.79	−45.56	11.70	0.53	9.16	9.94	12.70	−16.51	−19.13	32.88	101	16

although a little larger on the CIR than on the SEIR. The rotations constrain it to have occurred between Chrons 20o (42.8) and 20y (41.6), a period of only 1.2 Ma, in agreement with the topography of Dyment *et al.* (1999) which shows it occurring very abruptly around Chron 20o (42.8 Ma).

SWIR TRAJECTORIES AND SPREADING RATES

In Fig. 14 we show the predicted motion of four points on the Somalia Plate with respect to Antarctica (Som–Ant) along the SWIR. For clarity, as in Fig. 12, we only show the motion for two of the rotation sets ('With SWIR FZs' and 'With Carlsberg'; 2 and 3) and we omit the uncertainty ellipses. In Fig. 15 we zoom in on the central part of the trajectory starting at 40°S, 45°E and show trajectories for all four rotation sets with their confidence ellipses. As for the Cap–Som and Cap–Ant trajectories, the trajectory based on data set 1 ('Basic') flips back and forth around the smoother trajectories based on the other data sets. The trajectory constrained by the SWIR FZs (data set 2) is the smoothest and has the smallest uncertainty ellipses. The trajectory constrained only with the Carlsberg data (data set 3) zigzags back and forth for anomalies 20y to 22o, although within the uncertainties of the other trajectories, and then deviates from the other trajectories prior to anomaly 22o. This difference is significant for anomaly 24o and becomes larger for anomalies 25y and 26y. The trajectory based on rotation set 4 ('All') is also smooth but does not follow as sharp a curve prior to anomaly 24o as the trajectory based on rotation set 2 ('With SWIR FZs'). Thus, as with the Cap–Som and Cap–Ant trajectories, the Som–Ant trajectories reflect the divergence in poles prior to anomaly 22o between rotation sets constrained with and without Carlsberg data. It is important to note that the characteristic and uncommon continuous change of direction of the SWIR fracture zones before anomaly 20 is already obtained with data set 1 which does not use any constraints from SWIR fracture zones, themselves.

The record of spreading rate changes on the SWIR is shown in the inset in Fig. 15. The uncertainty in spreading rate on the SWIR varied between 10 and 30 per cent. The spreading rates are more poorly constrained than on the CIR and SEIR due to the

Table 4. Finite rotations for data set 3 ('With Carlsberg').

Anom	Lat. (°N)	Long. (°E)	Angle (°)	$\hat{\kappa}$	a	b	c	d	e	f	Points	Segs
						Antarctica–Africa						
20y	−16.29	−150.71	24.71	0.84	3.54	12.22	55.35	−4.40	−21.17	9.95	113	13
20o	−16.49	−151.56	25.31	0.67	2.21	9.11	52.85	−3.25	−19.30	8.75	132	13
21y	−15.53	−152.59	26.78	0.46	2.09	6.31	26.84	−2.43	−10.52	6.20	124	13
21o	−14.74	−153.12	28.06	1.64	2.33	7.65	33.35	−2.70	−11.98	5.81	130	13
22o	−14.51	−155.35	29.60	1.35	4.31	17.99	85.31	−5.97	−28.79	12.32	115	11
23o	−14.04	−157.45	31.92	0.81	2.80	10.29	47.43	−3.11	−14.32	6.08	130	13
24o	−14.56	−160.30	33.73	0.77	3.17	10.28	44.16	−2.97	−13.07	5.76	104	11
25y	−14.38	−163.27	36.58	0.39	8.51	33.59	151.17	−8.93	−40.99	13.40	78	10
26y	−14.65	−164.95	38.29	1.12	8.34	33.77	156.97	−8.22	−39.15	11.75	76	9
						Capricorn−Somalia						
20y	−17.18	−132.11	23.15	0.84	7.77	21.43	63.91	−5.92	−17.64	6.02	113	13
20o	−17.50	−132.54	23.60	0.67	6.69	20.93	70.00	−6.62	−21.15	8.06	132	13
21y	−17.14	−133.33	24.64	0.46	3.67	8.74	24.09	−2.47	−6.19	3.05	124	13
21o	−17.02	−134.13	25.75	1.64	3.51	9.77	30.14	−2.83	−8.09	3.92	130	13
22o	−17.34	−136.74	26.79	1.35	9.00	28.77	97.16	−7.19	−23.99	7.64	115	11
23o	−17.30	−139.73	28.54	0.81	4.30	13.00	42.53	−3.20	−10.20	4.16	130	13
24o	−17.85	−142.99	29.93	0.77	3.99	10.60	31.60	−2.66	−7.46	3.64	104	11
25y	−18.90	−147.36	31.87	0.39	8.62	22.44	63.31	−4.89	−13.42	5.00	78	10
26y	−19.58	−149.76	33.15	1.12	9.59	25.16	73.34	−4.39	−12.87	4.54	76	9
						Antarctica–Somalia						
20y	11.86	−42.51	7.53	0.84	5.40	4.80	5.05	−2.52	−2.87	6.03	113	13
20o	11.95	−42.67	7.87	0.67	5.65	5.14	5.59	−3.24	−3.67	5.31	132	13
21y	11.22	−41.11	8.49	0.46	5.40	5.51	6.64	−4.38	−5.08	7.82	124	13
21o	9.81	−40.73	8.83	1.64	5.68	6.12	7.71	−5.80	−6.57	9.83	130	13
22o	9.28	−40.41	9.21	1.35	8.43	9.95	13.33	−7.98	−9.75	13.40	115	11
23o	9.12	−39.96	9.62	0.81	8.89	10.13	13.59	−10.00	−11.94	15.38	130	13
24o	10.07	−41.50	9.99	0.77	11.29	11.71	14.08	−12.88	−14.12	19.62	104	11
25y	7.69	−39.86	10.43	0.39	42.87	51.32	64.43	−58.22	−72.59	88.73	78	10
26y	7.12	−39.72	10.67	1.12	44.80	52.08	62.96	−60.59	−73.58	93.16	76	9

much slower overall spreading history. For clarity, we dropped the point for anomaly 25y on these plots since the interval between 25y and 26y at the slow spreading rate, and with these errors, was too short to give a meaningful answer. However, it is clear that there is a gradual increase in spreading rates starting around Chron 24o or 23o and continuing until Chron 20o. The spike between Chrons 20o and 20y, another short time interval, is also probably an artefact.

MISFIT OF THE CARLSBERG RIDGE DATA PRIOR TO ANOMALY 22o

Perhaps the most unexpected result in this study is the divergence in the rotation poles prior to anomaly 22o for all three ridges depending on whether or not the data sets contain constraints from the Carlsberg Ridge. This shows up very clearly in Figs 8 and 9 showing the CIR and SEIR rotations. The rotations constrained by the Carlsberg Ridge data (data sets 3 and 4; 'With Carlsberg' and 'All') are very similar to the rotations constrained by data set 2 ('With SWIR FZs') for anomalies 20y, 20o, 21y, 21o and 22o. However, starting with anomaly 23o there is a progressively larger difference between rotations constrained with versus without the Carlsberg data. Although this is not completely unexpected for anomaly 26y, since spreading in the Mascarene Basin may have continued at a very slow rate after the main axis of India–Africa spreading jumped to the north side of the Seychelles around Chron 27 (Todal & Edholm 1998; Royer *et al*. 2002), it is surprising to see a difference in poles as young as Chron 23o.

The reason for the divergence in the rotation poles prior to anomaly 22o is apparent from Fig. 16 in which data points from the East Somali Basin (south flank of the Carlsberg Ridge) have been rotated back to their conjugate position in the Arabian Basin using rotations from data set 2 ('With SWIR FZs'). The covariance matrices associated with these rotations are used to calculate uncertainty ellipses for each of these rotated points. There is very good agreement between the rotated and fixed positions of anomalies 20y to 22o. This good agreement argues against the misfit being due to a poorly constrained Neogene (anomaly 6no) Capricorn–India rotation. However, starting with anomaly 23o, anomaly picks on the Carlsberg Ridge have a larger-than-predicted separation, increasing to over 100 km for anomaly 26y. The sense of this misfit is unexpected since, if the reason for the misfit is due to spreading between India and Africa that occurred on another subparallel ridge, for example, in the Mascarene Basin or the Gop Basin (Yatheesh *et al*. 2009), then one would measure a smaller-than-predicted separation across the Carlsberg Ridge. The sense of the misfit, instead, requires that there is a similar amount of previously unrecognized convergence somewhere in the plate circuit linking the Somalia, India and Capricorn plates.

We note that we can rule out the misfit being due to some missing plate motion outside of the Somalia–India–Capricorn Plate circuit (i.e. in the Somalia–India–Antarctic Plate circuit) because the rotations for the CIR and SEIR constrained with data sets 1 and 2, excluding Carlsberg data, agree very well with the rotations determined by Patriat (1987) and Royer & Sandwell (1989) for the CIR and SEIR based on two-plate solutions. It is very unlikely that

Table 5. Finite rotations for data set 4 ('All').

Anom	Lat. (°N)	Long. (°E)	Angle (°)	$\hat{\kappa}$	a	b	c	d	e	f	Points	Segs
						Antarctica–Africa						
20y	−16.33	−150.75	24.71	0.93	3.50	11.80	49.07	−4.20	−18.03	8.37	133	18
20o	−16.61	−151.68	25.28	0.78	2.18	8.55	43.10	−2.99	−14.87	6.75	162	18
21y	−15.50	−152.58	26.77	0.55	1.98	6.25	26.52	−2.51	−10.33	5.95	154	18
21o	−14.75	−153.12	28.06	1.86	2.19	7.52	32.93	−2.74	−11.83	5.69	160	18
22o	−14.39	−155.24	29.63	1.40	4.12	16.70	75.87	−5.39	−24.34	10.20	145	16
23o	−13.95	−157.38	31.91	0.69	2.40	8.96	40.88	−2.73	−12.21	5.21	160	18
24o	−14.47	−160.25	33.68	0.55	2.72	9.13	38.68	−2.72	−11.35	5.13	134	16
25y	−14.89	−163.94	36.29	0.31	5.40	20.61	93.41	−5.72	−26.05	9.56	108	15
26y	−15.25	−165.72	37.97	0.44	5.11	19.40	89.02	−4.83	−22.52	7.62	106	14
						Capricorn–Somalia						
20y	−17.24	−132.14	23.12	0.93	4.95	14.16	45.17	−4.11	−12.97	4.85	133	18
20o	−17.71	−132.64	23.50	0.78	3.31	10.75	39.39	−3.59	−12.01	5.34	162	18
21y	−17.06	−133.30	24.69	0.55	2.38	5.98	18.18	−1.82	−4.83	2.74	154	18
21o	−17.03	−134.13	25.74	1.86	2.51	7.17	23.47	−2.26	−6.63	3.59	160	18
22o	−17.22	−136.65	26.87	1.40	4.87	16.39	59.94	−4.45	−15.75	5.81	145	16
23o	−17.00	−139.50	28.77	0.69	2.67	8.34	28.98	−2.25	−7.44	3.45	160	18
24o	−17.54	−142.75	30.18	0.55	2.74	7.67	24.83	−2.16	−6.32	3.42	134	16
25y	−18.19	−146.81	32.36	0.31	5.02	13.85	43.00	−3.09	−9.20	3.92	108	15
26y	−18.73	−149.02	33.79	0.44	4.93	13.64	43.94	−2.43	−7.92	3.47	106	14
						Antarctica–Somalia						
20y	11.84	−42.32	7.53	0.93	2.36	1.91	2.31	−2.28	−2.63	5.98	133	18
20o	11.84	−42.16	7.87	0.78	1.64	1.23	1.79	−1.95	−2.42	4.97	162	18
21y	11.29	−41.54	8.49	0.55	1.89	1.60	2.24	−2.76	−3.25	6.86	154	18
21o	9.82	−40.70	8.83	1.86	2.26	1.98	2.67	−3.69	−4.00	8.38	160	18
22o	9.19	−40.63	9.21	1.40	2.73	2.54	3.70	−4.70	−5.40	10.84	145	16
23o	9.46	−41.49	9.64	0.69	2.83	2.78	4.20	−4.57	−5.37	9.48	160	18
24o	10.40	−43.28	9.99	0.55	4.68	4.36	5.68	−7.46	−7.65	13.92	134	16
25y	11.06	−46.04	10.59	0.31	9.83	11.38	15.87	−17.15	−21.78	34.35	108	15
26y	11.24	−47.20	10.85	0.44	9.59	10.89	14.27	−16.13	−20.17	32.51	106	14

there could be missing plate motion in the Somalia–India–Capricorn Plate circuit and still have the three-plate solutions agree with the two-plate solutions for these two ridges.

MISSING CONVERGENCE IN THE SOMALIA–INDIA–CAPRICORN PLATE CIRCUIT

The missing convergence within the Somalia–India–Capricorn Plate circuit prior to Chron 22o might have occurred either within the African (Somali) or Indian Plate. If it occurred within the Somali Plate, the most likely location of a missing boundary is probably across the Amirante Ridge-Trench structure, the enigmatic feature speculated to have been a convergent boundary in the late Cretaceous and earliest Cenozoic (Fisher *et al*. 1968; Miles 1982; Masson 1984; Mart 1988; Dyment 1991; Bernard & Munschy 2000). This feature was thought to have been active mainly in the late Cretaceous based on a single radiometric age of 82 Ma measured by Fisher *et al*. (1968). However, Stephens *et al*. (2009) analysed more recently acquired dredge samples from the Amirante Ridge and obtained a radiometric date of 52 Ma on a fresh gabbro, which is very close to the end of the period of missing plate motion. Alternatively, if the missing plate motion occurred within the Indian Plate there are no obvious candidates for where the boundary may have been located. To suggest two places, we note that the motion could have been accommodated either by a short-lived convergent boundary along the western margin of India or by a deformation zone east of the Chagos–Laccadive Ridge in the approximate location of the current India–Capricorn diffuse plate boundary. Such a 'proto' India–Capricorn deformation zone would be difficult to detect since it would have developed in young, thinly sedimented crust, and then would have been buried beneath the thick Neogene sediments coming from the Himalayas and, finally, overprinted by the current India–Capricorn convergent motion.

We can quantify the amount of missing motion in the Somalia–India–Capricorn Plate circuit by summing our best CIR rotations that do not use the Carlsberg Ridge constraints (rotation set 2, 'With SWIR FZs') with the rotations of Royer *et al*. (2002), which are based only on Carlsberg Ridge data. This analysis requires some background discussion because of another long-term problem, which is the difficulty of fitting the Indian Plate back to Africa across the Carlsberg Ridge parallel to the isochrons, due to the lack of good fracture zone offsets in the Arabian Basin and East Somali Basin. As noted in the background section, Molnar *et al*. (1988) used the fit of the Chagos Ridge to the Mauritius FZ and the Chain Ridge to the Owen Ridge as a major constraint on the fit of India and Africa. The more recent work of Royer *et al*. (2002) used detailed surveys (Chaubey *et al*. 2002) of the magnetic anomalies and propagators in the Arabian Basin and East Somali Basin to constrain a revised alignment of features in the two basins. The rotations of Royer *et al*. (2002) moved Africa about 60 km to the west relative to India in reconstructions of anomalies 20 to 26 compared to the rotations of Molnar *et al*. (1988).

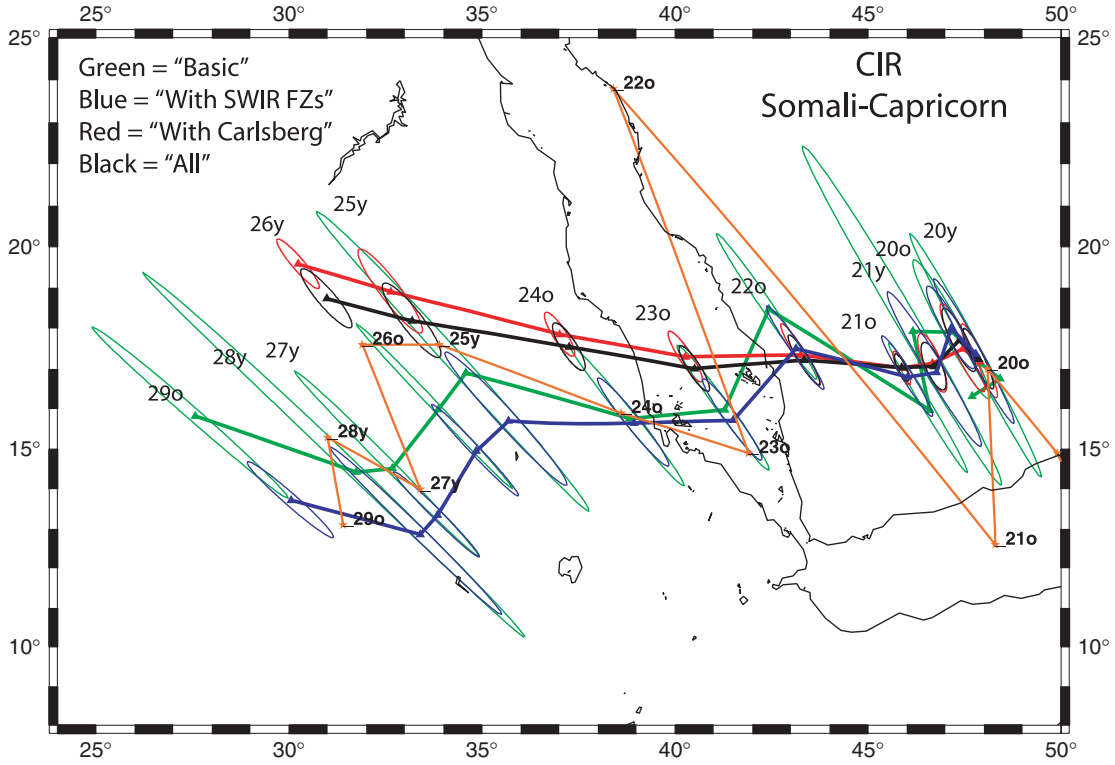

Figure 8. Euler poles, with their 95 per cent confidence ellipses, for the CIR for the four rotation sets described in the text. Note that the Euler poles that include Carlsberg Ridge constraints (sets 3 and 4: 'With Carlsberg' and 'All') diverge from the other two sets of Euler poles prior to anomaly 22o. Gold stars connected by the gold line show Euler poles of Patriat (1987).

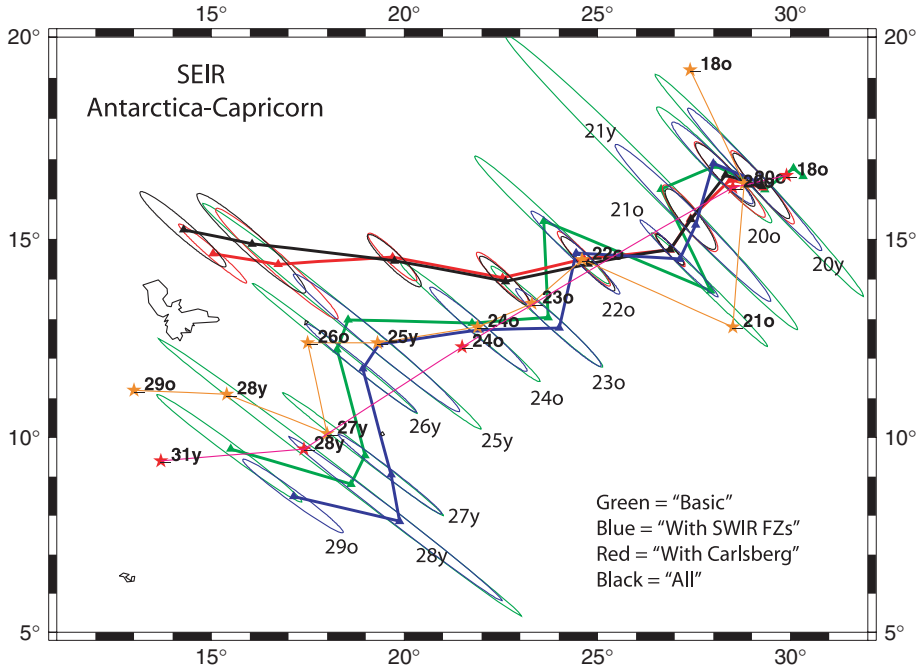

Figure 9. Euler poles, with their 95 per cent confidence ellipses, for the SEIR for the four rotation sets described in the text. Note that the Euler poles that include Carlsberg Ridge constraints (sets 3 and 4: 'With Carlsberg' and 'All') diverge from the other two sets of Euler poles prior to anomaly 22o. Gold stars connected by the gold line show Euler poles of Patriat (1987), red stars connected by a red line show Euler poles of Royer & Sandwell (1989).

Our work shows that this issue is still unresolved. This is apparent in Fig. 17 in which we compare different sets of Somalia–India (Som–Ind) rotations. We first calculated Som–Ind rotations based on our data constraints by summing the 'With SWIR FZs' (data set 2) Som–Cap (CIR) rotations with the anomaly 6no Cap–Ind rotation of DeMets *et al*. (2005). The comparison of our Som–Ind rotations to the Royer *et al*. (2002) Som–Ind rotations in Fig. 17 shows that these two sets of rotations do not agree even for anomalies 20o,

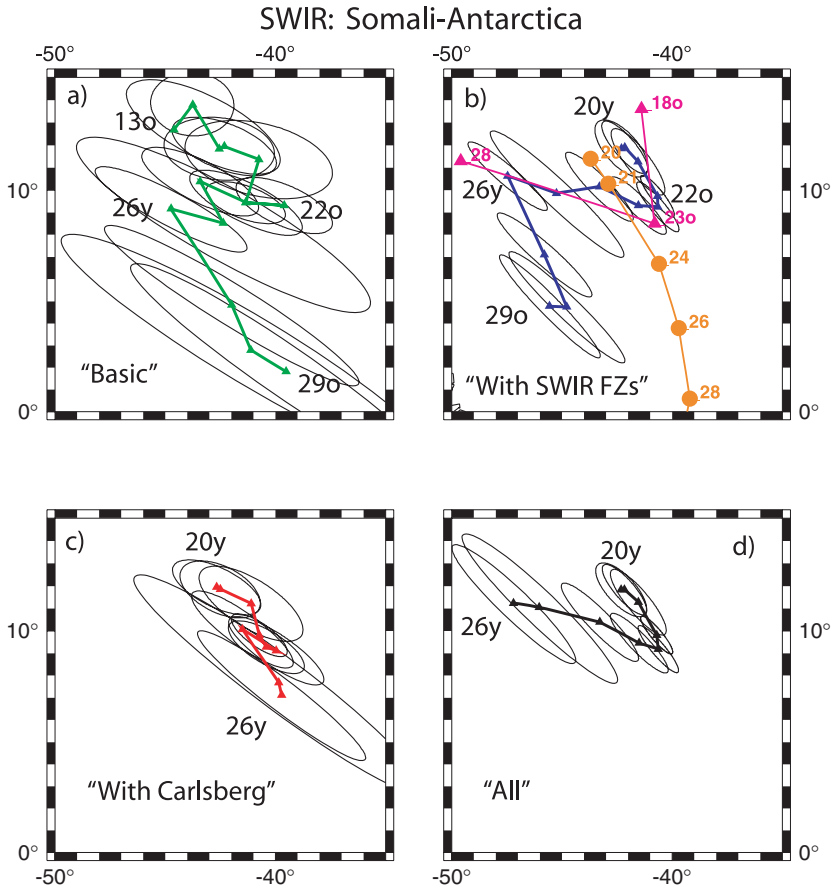

Figure 10. (a)–(d) Euler poles, with their 95 per cent confidence ellipses, for the SWIR for the four rotation sets described in the text. The smoothest progression of Euler poles is for rotation set 2 ('With SWIR FZs') shown in (b). In (b) gold circles show the poles of Royer *et al*. (1988), purple triangles show Bernard *et al*. (2005).

21y, 21o and 22o, a period when the four sets of Som–Cap rotations calculated in this paper agree with each other. The sense of the discrepancy in terms of plate motion shows up well in a comparison of Som–Ind trajectories based on the rotations of Royer *et al*. (2002), Molnar *et al*. (1988) and our 'With SWIR FZs' Som–Ind rotations. Fig. 18 shows a point on the Somali Plate rotated back to the Indian Plate for several time steps and for these three sets of rotations. The points rotated by the 'With SWIR FZs' Som–Ind rotations fall about 60 km east of the Royer *et al*. (2002) constrained points for anomalies 20y to 22o. Interestingly, they also fall along the same line as points rotated by the Molnar *et al*. (1988). We only plotted trajectories based on the 'With SWIR FZs' rotations back to anomaly 22o because of the pre-anomaly 22o missing plate motion problem.

The difference between the Royer *et al*. (2002) rotations and the 'With SWIR FZs' Som–Ind rotations between anomalies 20y and 22o could be due to some additional unrecognized motion within the Indian–Capricorn–Somali Plate circuit between anomalies 20y and 6no, but it more likely reflects difficulties in properly aligning the Somali and Indian plates across the Carlsberg Ridge since the misfits are parallel to the isochrons. We demonstrate this in Fig. 19 in which we show the anomaly 22o picks on the Somali Plate rotated back to the Arabian Plate using both the Royer *et al*. (2002) anomaly 22o rotation and the 'With SWIR FZs' Som–Ind anomaly 22o rotation. We have highlighted three of these points, showing the uncertainty ellipses for the points rotated by the 'With SWIR FZs' rotations. The Royer *et al*. (2002) pole rotates the East Somali Basin points about 60 km to the west of the 'With SWIR FZs' rotation. The misfit appears to be a simple sliding-along-the-isochron problem since both rotations are consistent with all of the magnetic anomaly picks.

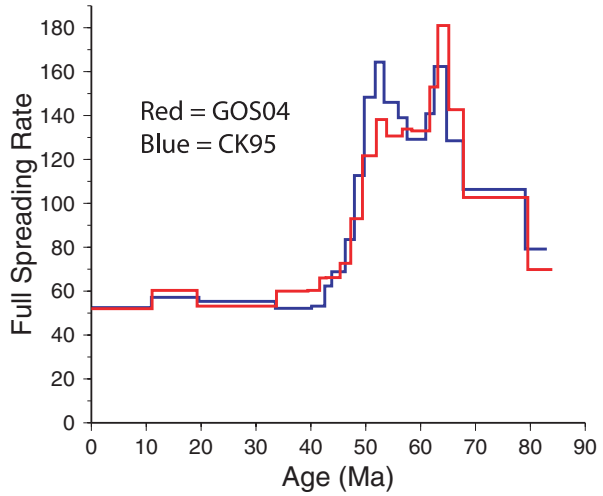

Figure 11. Comparison of spreading rates on the SEIR for a trajectory starting at 0°S, 85°E constrained by rotation set 2 ('With SWIR FZs') for two different magnetic polarity timescales: CK95 and GOS04. The GOS04 timescale leads to a smoother set of spreading rate variations in the early Cenozoic and is used throughout this study.

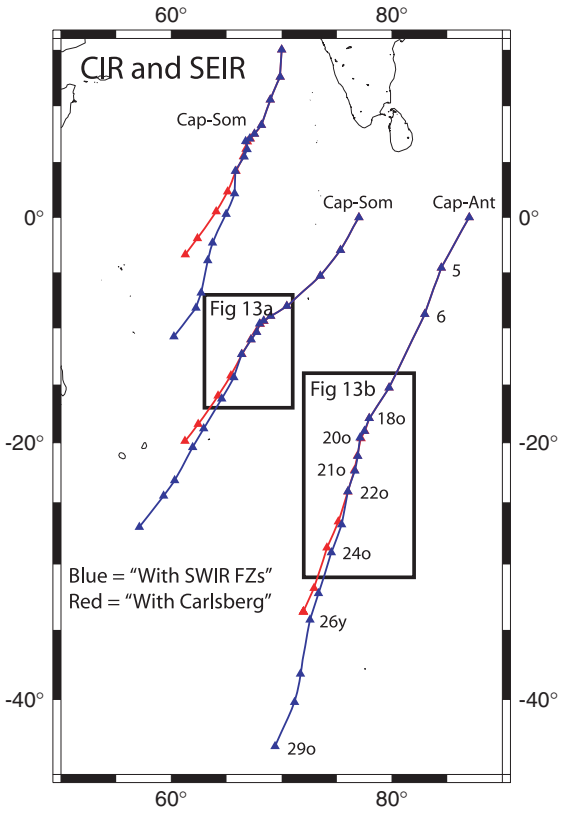

Figure 12. Trajectories for two representative Cap–Som points and one Cap–Ant point for rotation set 2 ('With SWIR FZs', blue) and rotation set 3 ('With Carlsberg', red). Note that the trajectories diverge prior to anomaly 22o.

ANOMALY 26y to 22o STAGE POLES FOR THE MISSING MOTION

Since the difference between the Royer *et al*. (2002) rotations and the 'With SWIR FZs' Som–Ind rotations for anomalies 22o and younger appears to be due to a simple and uniform misalignment, we decided to use the Royer *et al*. (2002) rotations to quantify the missing plate motion in the Somalia–Capricorn–India Plate circuit between anomalies 26y and 22o with the caveat that there is an offset corresponding to the along-isochron sliding. We did this both assuming the extra plate motion is within the Somalia Plate and assuming it is within the Indian Plate. We quantify the amount of convergence within the Somali Plate (e.g. across the Amirante Trench) by summing the Royer *et al*. (2002) Som–Ind rotations, the DeMets *et al*. (2005) Ind–Cap anomaly 6no rotation and the Cap–Som rotations based on data set 2 ('With SWIR FZs') to calculate motion within the Somali Plate (Table 6). If we assume the motion is across the Amirante Trench and represents convergence between a Seychelles microplate and the main Somali Plate (Fig. 20) then the rotations represent finite rotations for the motion of the Seychelles microplate relative to Somalia (Sey–Som). We combine the two Sey–Som finite rotations (anom 26y inv + anom 22o) to determine a stage pole for the forward motion of the Seychelles microplate relative to Somalia between anomalies 26y and 22o (Table 7) (heavy red ellipse, large red diamond in Figs 5 and 20). This stage pole predicts 110 km of convergence across the Amirante Trench and 180 km of convergence across the northern extension of this boundary between Chrons 26y to 22o. Estimates of this motion, with 95 per cent confidence limits based on the covariance matrix, are shown by the small red lines and small red ellipses in Figs 5 and 20. In our interpretation, the anomaly 22o Sey–Som finite rotation represents the motion due to the 'along-isochron sliding' issue with the Royer *et al*. (2002) rotations that we noted earlier.

Alternatively, we calculated rotations assuming the missing convergent motion in the Somalia–Capricorn–India Plate circuit took place within the Indian Plate by summing the same rotations, but in a slightly different order: India–Capricorn, Capricorn–Somalia and Somalia–India (Table 6). These rotations represent the motion of the more southeasterly part of the Indian Plate (Ind2) relative to the more northwesterly part of the Indian Plate (Ind1). As for the Somali Plate case, we combined the anom 26y and 22o rotations (anom 26y inv + anom 22o) to determine a stage pole for the forward motion of Ind2 relative to Ind1 between anomalies 26y and 22o (Table 7). The stage pole (heavy blue ellipse, large blue diamond in Figs 5 and 20) predicts about 100 to 200 km of convergence on the seafloor either along the western margin of India or along a proto-India–Capricorn deformation zone southeast of India (light blue lines and small blue ellipses in Figs 5 and 20).

It is interesting to note that in both cases (motion within the African Plate or motion within the Indian Plate) the anom 26y to 22o stage pole was located over the then-active part of the long north–south transform boundary linking the southern part of the CIR to the Carlsberg Ridge: relative to the Somali Plate it lies over the Mauritius FZ (red ellipse, red diamond, Fig. 20) and relative to the Indian Plate it is over the middle part of the Chagos–Laccadive Ridge (blue ellipse, blue diamond, Fig. 20). At this time the Reunion hotspot was also beneath the active part of the transform boundary. In fact, coincidentally, Deep Sea Drilling Project site 517, with an age of 56.6 Ma, is located very close to the anom 26y to 22o stage pole relative to the Indian Plate (Fig. 5).

Of the three alternative locations for accommodating missing plate motion in the plate circuit that we present here, we believe the two west of the CIR (a separate Seychelles microplate or convergence along the western Indian margin) are the most probable. The presence of the Reunion hotspot beneath the long transform boundary linking the CIR to the Carlsberg Ridge would weaken that boundary and might enable the development of independent motion across a convergent zone radiating away from the Chagos–Laccadive Ridge. The Seychelles microplate option is a particularly strong candidate. Gravity modelling (Miles 1982) indicates that the Amirante Trench was likely the site of some subduction although the extent of subduction is not clear. Although Stephens *et al*. (2009) reported that the samples in the dredge hauls from the Amirante Ridge that they analysed do not appear to be arc related, their radiometric age (52 Ma) corresponds very closely to the time of the cessation of motion (anomaly 22o). One potential problem is that the Amirante structure ends around 6°S, 53°E while a distinct microplate that existed until Chron 22o would have extended to about 5°N (Figs 5 and 20). Although there is no obvious fossil plate boundary north and west of the Amirante Trench, the rotations predict more, not less, convergence in this region. We speculate that the motion was distributed over a broad diffuse boundary, which, at the time it was deforming, would have been in relatively young oceanic crust and therefore did not leave a prominent gravity or topographic signature. Although we have not considered driving forces, we note that the kinematics of our model has similarities with the model of Mart (1988) in which he proposed that accretion between the Seychelles and India caused the Seychelles block to converge with the northern Mascarene Basin in the Palaeocene and Eocene.

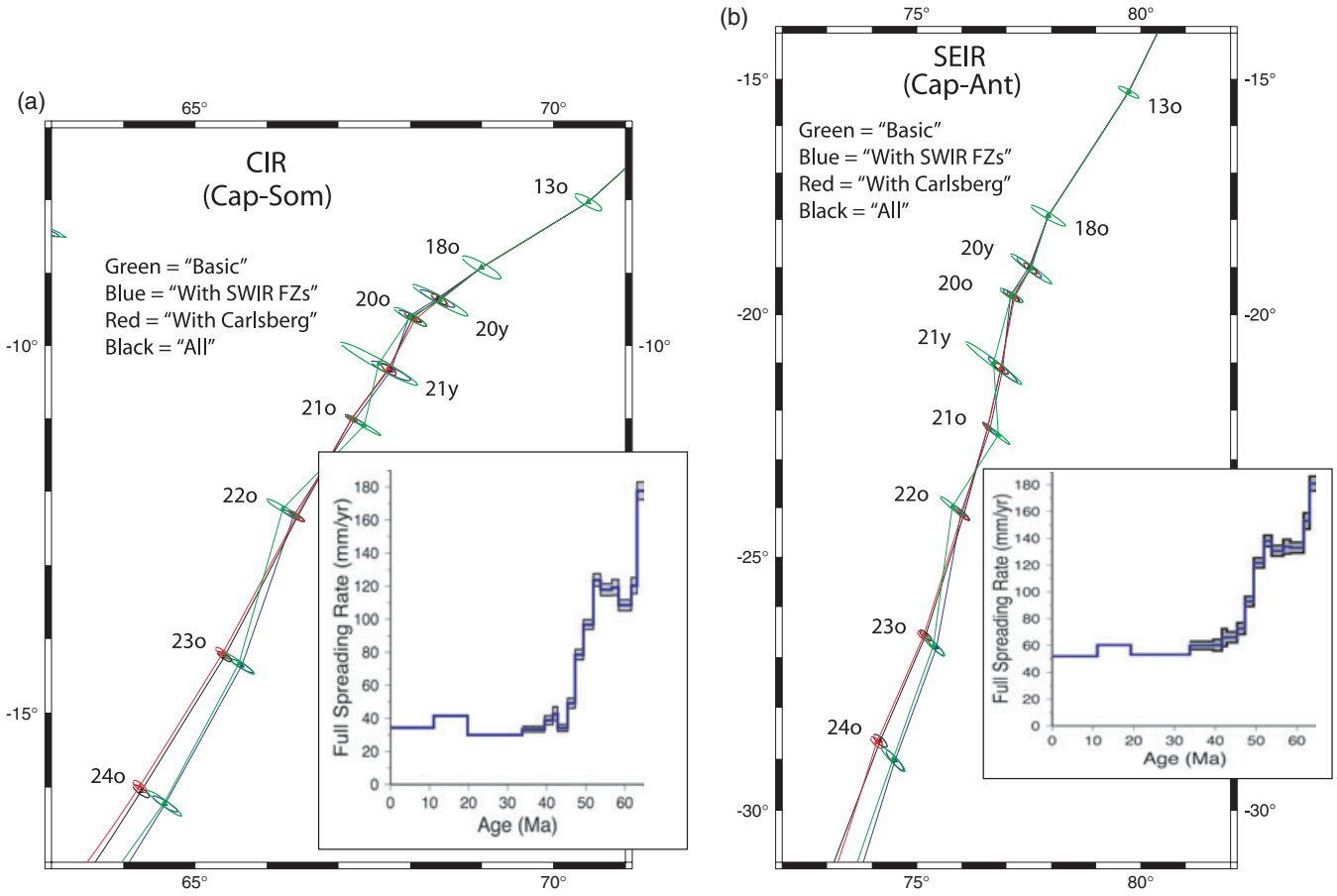

Figure 13. Enlargements of Fig. 12 showing (a) Cap–Som and (b) Cap–Ant trajectories for all four rotation sets. Ellipses show 95 per cent confidence zones. Insets show the spreading rate along these trajectories for rotation set 2 ('With SWIR FZs'). The spreading rate starts to slow at Chron 23o and decreases continuously until Chron 21y in both trajectories. The change in azimuth is abrupt at Chron 20o.

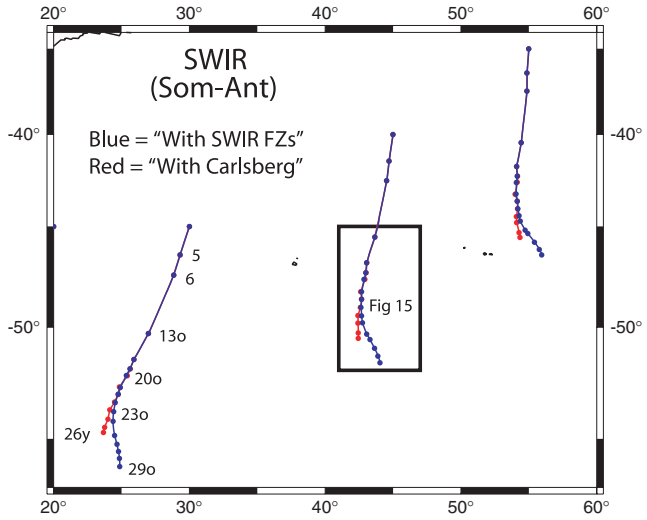

Figure 14. Som–Ant trajectories for rotation set 2 ('With SWIR FZs', blue) and rotation set 3 ('With Carlsberg', red). Note that the trajectories diverge prior to anomaly 23o.

It is important to determine the location of the missing plate motion. If it occurred within the Somali Plate or along the western continental margin of India, then India–Somalia rotations based solely on Carlsberg Ridge data (e.g. Royer *et al*. 2002) will not reflect true India–Somali motion prior to Chron 22o. Alternatively, if the motion occurred within the Indian Plate east of the Chagos–Laccadive Ridge, then the Capricorn–Somali rotations that we have calculated in this study do not reflect India–Somali motion prior to Chron 22o.

IMPLICATIONS

A future task, beyond the scope of this paper, is to sum our revised Capricorn–Somalia Plate rotations with the plate circuit linking the African, North American and Eurasian plates and derive updated motions for India with respect to Eurasia. This is not a trivial step since the best constrained rotations available for the Africa–North America (Müller *et al*. 1999) and North America–Eurasia (Gaina *et al*. 2002) are not at the same time intervals as the ones we report here and, just as troublesome, some of the Africa–North America rotations are not at the same time intervals as the North America–Eurasia rotations. Consequently, calculating rotations at the level of detail as we do here (roughly every 2 Ma) requires interpolating between these other rotations and these interpolations tend to produce abrupt, short period, changes in motion which are artefacts of the interpolations.

Nonetheless, our study has implications for the India–Eurasia collision. First, the slowdown in Capricorn–Somalia motion between anomalies 23o and 21y is so large that it will be mirrored in India–Eurasia motion and thus date the India–Eurasia slowdown.

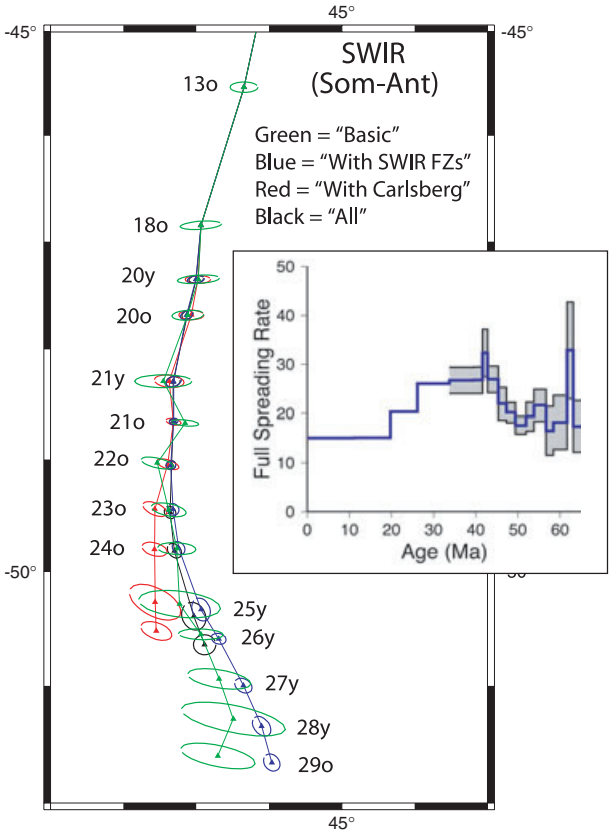

Figure 15. Enlargement of Fig. 14 showing Som–Ant trajectories for all four rotation sets. Ellipses show 95 per cent confidence zones. Inset shows the spreading rate along this trajectory for rotation set: 2 ('With SWIR FZs'). The spreading rate increases continuously between anomalies 23o and 20o. The trajectory based on rotation set 3 ('With Carlsberg', red) does not follow the bend in the Bain FZ around anomaly 23o.

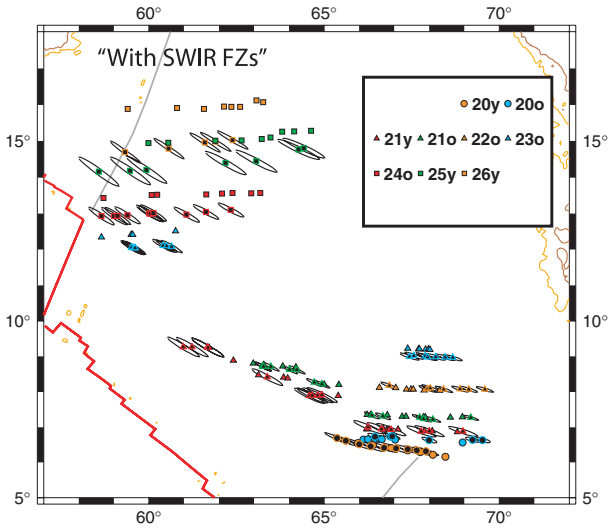

Figure 16. Demonstration of the progressively larger misfit of rotated points on the Carlsberg Ridge prior to anomaly 22o. Magnetic anomaly picks from the East Somali Basin are rotated back to the Arabian Basin using the Somali–Capricorn rotations based on set 2 ('With SWIR FZs'). Rotated points have coloured rims with black cores and have uncertainty ellipses drawn around them. The 'fixed' Arabian Basin data points have been corrected for India–Capricorn motion.

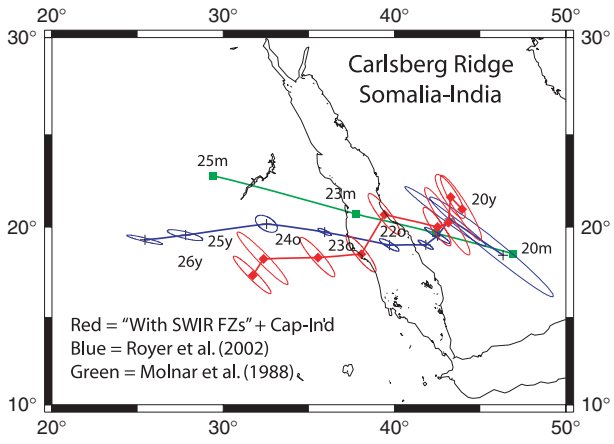

Figure 17. Comparison of three sets of Som–Ind rotations for anomalies 20y to 26y. Blue symbols are from Royer *et al*. (2002), green squares are from Molnar *et al*. (1988) and red diamonds are derived by summing the 'With SWIR FZs' Som–Cap rotations with the DeMets *et al*. (2005) anomaly 6no Cap–Ind rotation. Note that the Royer *et al*. (2002) rotations fall south of the 'With SWIR FZs' rotations for anomalies 22o and 21o, reflecting the 'along-isochron' sliding problem.

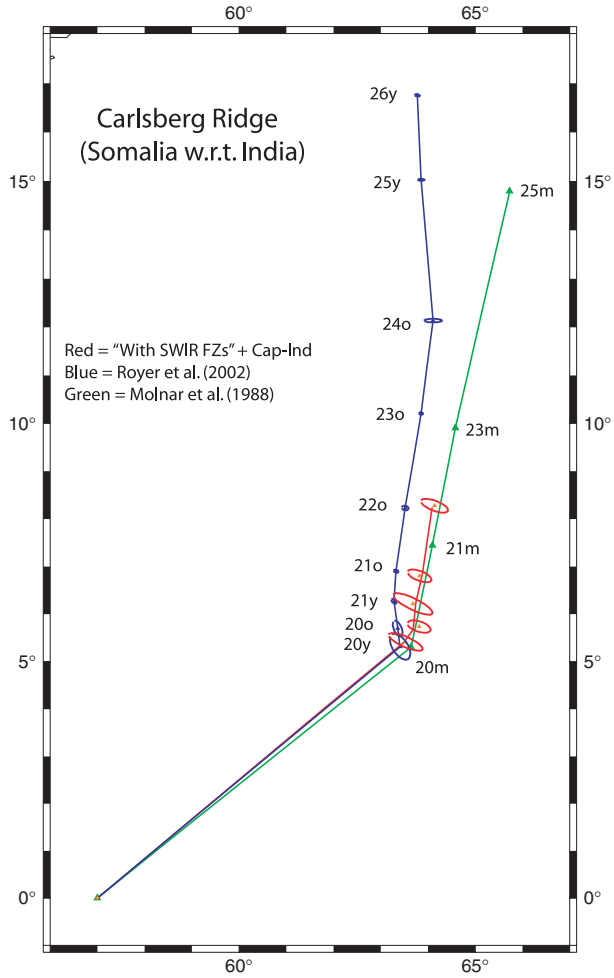

Figure 18. Trajectories of a point on the Somalia Plate relative to the Indian Plate for the three sets of Somali–India rotations in Fig. 17. Note that the trajectory based on the Royer *et al*. (2002) rotations lies about 60 km west of the trajectory based on the 'With SWIR FZs' rotations for anomalies 20o to 22o.

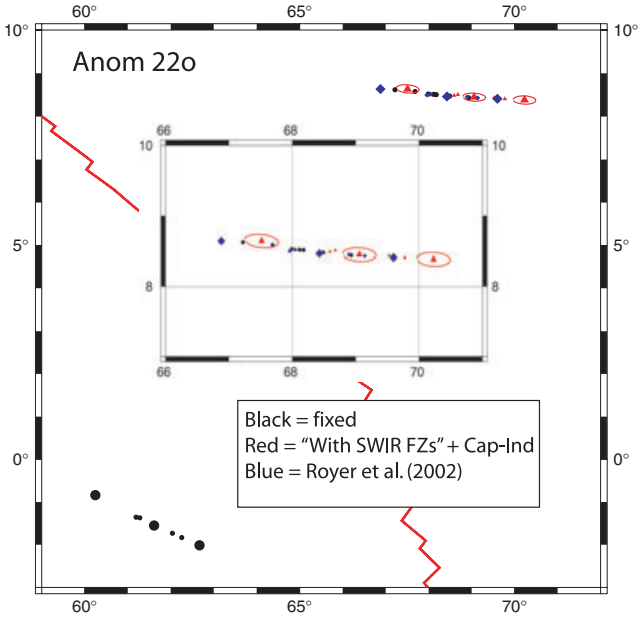

Figure 19. Illustration of the 'along-isochron' sliding problem on the Carlsberg Ridge described in text. Magnetic anomaly 22o picks from the East Somali Basin (black circles) have been rotated back to the Arabian Basin by both the Royer *et al*. (2002) Som–Ind rotation (blue diamonds) and the 'With SWIR FZs' Som–Ind rotation (red triangles). Both sets of rotated points align well with the Arabian Basin fixed points (black circles). However, points rotated by Royer *et al*. (2002) rotations are located about 60 km west of the points rotated by the 'With SWIR FZs' Som–Ind rotations. Larger symbols highlight three selected points. Inset is an enlargement of the north side.

The slowdown started around anomaly 23o (51.9 Ma). Second, our study points out the importance of determining the location of the deformation in the India–Capricorn–Somalia Plate circuit prior to Chron 22o since Capricorn–Somalia has a kink in the direction of relative motion at Chron 22o that is much larger than observed in India–Somalia motion. Thus, depending on the location of the convergence (i.e. whether it is east or west of the CIR) the smoothness of the India–Eurasia trajectory will differ at Chron 22o. It is also intriguing that this period of deformation ended at Chron 22o, the time of the India–Eurasia slowdown.

The relationship to coeval tectonic events in the Pacific Ocean has been the object of speculation for a considerable time (e.g. Patriat & Achache 1984; Norton 1995). The initiation of the Somalia–Capricorn slowdown at 23o is coeval with major changes in spreading direction on the Pacific–Farallon and Pacific–Kula Ridges (Atwater 1989). However it is not known if these tectonic events are related in some way to the Indian Ocean events or if they reflect a more regional Pacific Basin event such as the subduction of the Pacific–Izanagi Ridge (Whittaker *et al*. 2007). We note that the recent compilation of radiometric ages along the Hawaiian–Emperor chain by Sharp & Clague (2006) now identifies two distinct events in the development of the Bend in the Hawaiian–Emperor chain: the initiation of volcanism along the Hawaiian trend around 50 Ma and the onset of a faster rate of migration of volcanic activity, marking the completion of the Bend, around 42 Ma, roughly coincident with the times of the two major tectonic events in the Indian Ocean.

SUMMARY AND CONCLUSIONS

We calculated four sets of Euler rotations for the Capricorn, Somalia and Antarctic plates for 14 time intervals in the early Cenozoic (from anomaly 29o to anomaly 13o) using the Hellinger method as implemented by Royer & Chang (1991) and Kirkwood *et al*. (1999). Each set of rotations had a different combination of data constraints. The first set of rotations used a basic set of magnetic anomaly picks on the CIR, SEIR and SWIR and fracture zone constraints on the CIR and SEIR, but did not incorporate data from the Carlsberg Ridge and did not use fracture zones on the SWIR. The second set added fracture zone constraints from the region of the Bain fracture zone on the SWIR which were dated with synthetic flowlines based on the first data set. The third set of rotations used the basic constraints of the first data set plus data from the Carlsberg Ridge. The fourth set of rotations used both the SWIR fracture zone constraints and the Carlsberg Ridge constraints.

We found that the two sets of rotations constrained by the Carlsberg Ridge data diverged from the other two sets of rotations prior to anomaly 22o. This is because the separation of the magnetic anomalies on the Carlsberg Ridge is not consistent with rotations

Table 6. Finite rotations for the Capricorn–India–Somalia Plate circuit.

Anom	Lat. (°N)	Long. (°E)	Angle (°)	$\hat{\kappa}$	a	b	c	d	e	f
India–Capricorn (Ind–Cap)										
6no	−3.08	75.79	3.22	1.00	23.31	47.08	106.51	−1.47	−0.24	5.76
From DeMets *et al*. (2005)										
Somalia–India (Som–Ind)										
26y	19.30	25.44	30.58	9.13	748.62	1115.08	1670.13	−4.75	−1.52	5.81
22o	19.02	39.70	24.52	4.45	112.77	195.41	347.39	−5.64	−5.42	5.93
From Royer *et al*. (2002) and Royer (personal communication, 2009)										
Seychelles–Somalia (Sey–Som)										
26y	−8.69	64.39	−4.99	1.00	742.16	1102.29	1659.86	−110.05	−162.30	110.58
22o	−50.79	35.10	0.76	1.00	165.66	273.00	472.51	−45.44	−68.29	40.30
Summation of Som–Ind + Ind–Cap + Cap–Som (With SWIR FZs)										
India2 – India1 (Ind2 – Ind1)										
26y	11.50	74.20	−4.99	1.00	97.03	234.14	656.96	13.92	−3.53	37.92
22o	−45.62	69.07	0.76	1.00	47.34	117.41	329.66	−5.09	−21.47	19.91
Summation of Ind–Cap + Cap–Som (With SWIR FZs) + Som–Ind										

Table 7. Stage poles for missing convergent motion between anomalies 22o and 26y.

Anom	Lat. (°N)	Long. (°E)	Angle (°)	$\hat{\kappa}$	a	b	c	d	e	f
Seychelles–Somalia (Sey–Som) stage pole with Somalia Plate fixed										
26y–22o	−13.96	61.64	5.52	1.00	322.07	470.96	727.65	−154.88	−219.76	139.10
Forward motion (anom 26y inv + anom 22o)										
India2–India1 (Ind2–Ind1) stage pole with India1 fixed										
26y–22o	4.79	73.40	5.44	1.00	155.53	367.89	973.14	7.56	−16.99	60.15
Forward motion (anom 26y inv + anom 22o)										

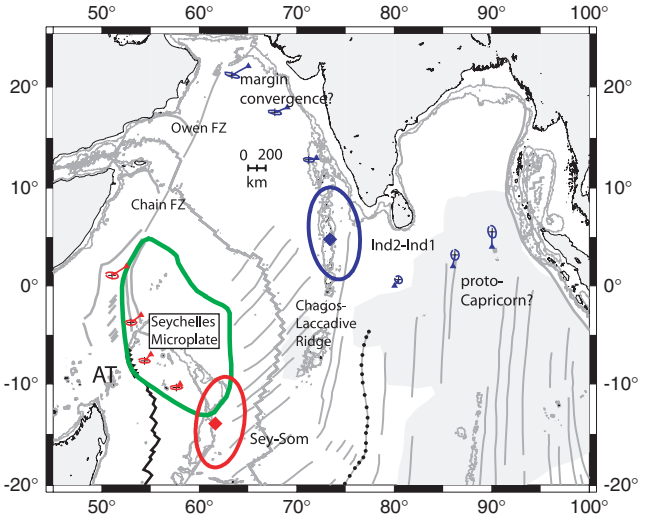

Figure 20. Three scenarios for accommodating missing convergent motion in the Somali–Capricorn–India Plate circuit prior to anomaly 22o. Scenario 1 (red lines and small red ellipses): convergence within the Somali Plate, for example, between a Seychelles microplate (green) and the main Somalia Plate. Motion within the Somali Plate was estimated by summing the plate circuit Som–Ind, Ind–Cap and Cap–Som. The heavy red ellipse and red diamond shows the location of the anomaly 26y to 22o stage pole for motion of the Seychelles microplate relative to the Somali Plate. Scenarios 2 and 3 (blue lines and small blue ellipses): convergence within the Indian Plate either along the western margin of India or within the Indian Plate east of the CIR. Motion within the Indian Plate was calculated by summing Ind–Cap, Cap–Som and Som–Ind. The heavy blue line and blue diamond shows the location of the anomaly 26y to 22o stage pole for the motion of the more southeasterly part of the Indian Plate (Ind2) relative to the more northwesterly part of the Indian Plate (Ind1).

for the CIR that fit all three branches of the IOTJ simultaneously prior to anomaly 22o. Instead, there is a progressively larger separation of anomalies on the Carlsberg Ridge, starting at roughly 25 km for anomaly 23o and increasing to over 100 km for anomaly 26y.

These data require an extended period of previously unrecognized slow convergence somewhere in the plate circuit linking the Indian, Capricorn and Somali plates during the period between Chrons 26y and 22o. The most likely location for the convergence is between a distinct Seychelles microplate and the main part of the Somali Plate in the region of the Amirante Trench. The sense of the misfit on the Carlsberg Ridge is consistent with roughly 100–150 km of convergence across a compressive boundary that included the Amirante Trench and which extended north to the Carlsberg Ridge axis at Chron 22. Northwest of the Amirante Trench this motion would have been accommodated across a broad zone of diffuse deformation. Alternatively, there may have been slow convergence within the Indian Plate, perhaps along the western margin of India or within the Indian Plate east of the CIR in the region of the current Capricorn–Indian diffuse plate boundary.

Between Chrons 20y and 22o, the rotations constrained by data set 4 ('All') should be the most accurate recorders of motion on all three ridges (SWIR, CIR and SEIR). The CIR Somali–Capricorn motion can be summed with the DeMets *et al*. (2005) anomaly 6no Capricorn–India rotation to get Somali–India motion. Prior to Chron 22o, the rotations constrained by data set 2 ('With SWIR FZs') should be the most accurate recorders of motion on the SWIR, SEIR and CIR. However, until the source of the missing plate motion within the Somali–India–Capricorn Plate circuit prior to Chron 22o is resolved, it is not clear if the Somali–Capricorn motions summed with anomaly 6no Capricorn–India motion represents true Somali–India motion.

Our work sharpens the dating of the two major Eocene events that Patriat & Achache (1984) recognized in the Indian Ocean: a large but gradual slowdown on the CIR and SEIR starting around Chron 23o (51.9 Ma) and continuing until Chron 21y (45.3 Ma), a period of 6.6 Ma, followed 2 or 3 Ma later by an abrupt change in spreading azimuth on the CIR and SEIR which occurred around Chron 20o (42.8) Ma and which was completed by Chron 20y (41.5 Ma). No change in spreading rate accompanied the abrupt change in spreading direction. These events are coeval with other major tectonic events in the Pacific, Indian and Atlantic Oceans.

ACKNOWLEDGMENTS

Helpful comments were received from Ian Norton and two anonymous reviewers. Support for this work was provided by NSF grant ANT0944345 to SCC. A stipend from IPGP to SCC supported an extended stay in Paris; stipends from SIO supported extended stays at Scripps by PP and JD. This is IPGP contribution #3043.

REFERENCES

Atwater, T., 1989. Plate tectonic history of the northeast Pacific and western North America, in *The Eastern Pacific Ocean and Hawaii, The Geology of North America*, Vol. N, pp. 21–72, eds Winterer, E.L., Hussong, D.M., Decker, R.W., Geological Society of America, Boulder, CO.

Bergh, H.W., 1971. Sea floor spreading in the southwest Indian Ocean *J. geophys. Res.,* **76,** 6276–6282.

Bergh, H.W. & Norton, I.O., 1976. Prince Edward fracture zone and the Evolution of the Mozambique Basin, *J. geophys. Res.,* **81,** 5221–5239.

Bernard, A. & Munschy, M., 2000. Le basin des Mascareignes et le basin de Laxmi (ocean Indien occidental) se sont-ils formes a l'axe d'un meme centre d'expansion? *Comptes Rendus del'Academie de Sciences Serie 2a,* **330,** 777–783.

Bernard, A., Munschy, M., Rotstein, Y. & Sauter, D., 2005. Refined spreading history at the Southwest Indian Ridge for the last 96 Ma, with the aid of satellite gravity data, *Geophys. J. Int.,* **162,** 765–778.

Cande, S.C. & Kent, D.V., 1995. Revised calibration of the geomagnetic polarity timescale for the Late Cretaceous and Cenozoic, *J. geophys. Res.,* **100,** 6093–6095.

Chang, T., 1987. On the statistical properties of estimated rotations, *J. geophys. Res.,* **92,** 6319–6329.

Chang, T., 1988. Estimating the relative rotation of two tectonic plates from boundary crossings, *J. Am. Stat. Assoc.,* **83,** 1178–1183.

Chaubey, A.K., Dyment, J., Bhattacharya, G.C., Royer, J.Y., Srinivas, K. & Yatheesh, V., 2002. Paleogene magnetic isochrons and palaeo-propagators in the Arabian and Eastern Somali basins, NW Indian Ocean, in *The Tectonic and Climatic Evolution of the Arabian Sea Region,* pp. 71–85, eds Clift, P.D., Croon, D., Gaedicke, C., Craig, J., Geological Society, London.

Chu, D. & Gordon, R.G., 1999. Evidence for motion between Nubia and Somalia along the Southwest Indian Ridge, *Nature,* **398,** 64–67.

DeMets, C., Gordon, R.G. & Argus, D.F., 1988. Intraplate deformation and closure of the Australia-Antarctica-Africa plate circuit, *J. geophys. Res.,* **93,** 11 877–11 897.

DeMets, C., Gordon, R.G. & Royer, J.-Y., 2005. Motion between the Indian, Capricorn, and Somalian plates since 20 Ma: implications for the timing and magnitude of distributed lithospheric deformation in the equatorial Indian Ocean, *Geophys. J. Int.,* **161,** 445–468.

Dyment, J., 1991. Structure et evolution de la lithosphere oceanique dans l'ocean Indien: apport des anomalies magnetiques, *PhD thesis*, Univ. Louis Pasteur, Strasbourg, France, 374 pp.

Dyment, J., 1993. Evolution of the Indian Ocean Triple Junction between 65 and 49 Ma (anomalies 28 to 21), *J. geophys. Res.,* **98,** 13 863–13 877.

Dyment, J., 1998. Evolution of the Carlsberg Ridge between 60 and 45 Ma: ridge propagation, spreading asymmetry, and the Deccan-Reunion hotspot, *J. geophys. Res.,* **103,** 24 067–24 084.

Dyment, J., Gallet, Y. & the Magofond 2 Scientific Party, 1999. The Magofond 2 cruise: a surface and deep tow survey on the past and present Central Indian Ridge, *Inter Ridge News,* **8,** 25–31.

Fisher, R.L., Engel, C.G. & Hilde, T.W.C., 1968. Basalts dredged from the Amirante Ridge, Western Indian Ocean, *Deep-Sea Res.*, **15,** 521–534.

Fisher, R.L., Sclater, J.G. & McKenzie, D.P., 1971. Evolution of the Central Indian Ridge, western Indian Ocean, *Geol. Soc. Am. Bull.,* **82,** 553–562.

Gaina, C., Roest, W.R. & Müller, R.D., 2002. Late Cretaceous-Cenozoic deformation of northeast Asia, *Earth planet. Sci. Lett.*, **197,** 273–286.

Gradstein, F.M., Ogg, J.G., Smith, A.G., Agterberg, F.P., Bleeker, W., Cooper, R.A., Davydov, V., Gibbard, P. *et al*., 2004. *A Geologic Time Scale 2004,* 589 pp, Cambridge Univ. Press, Cambridge, UK.

Haxby, W.F., 1987. Gravity field of the world's oceans (map), National Geophysical Data Center, NOAA, Boulder, Colorado.

Hellinger, S.J., 1981. The uncertainties of finite rotations in plate tectonics, *J. geophys. Res.,* **86,** 9312–9318.

Horner-Johnson, B.C., Gordon, R.G. & Argus, D.F., 2007. Plate kinematic evidence for the existence of a distinct plate between the Nubian and Somalian plates along the Southwest Indian Ridge, *J. geophys. Res.,* **112,** B05418, doi:10.1029/2006JB004519

Horner-Johnson, B.C., Gordon, R.G., Cowles, S.M. & Argus, D.F., 2005. The angular velocity of Nubia relative to Somalia and the location of the Nubia-Somalia-Antarctica triple junction, *Geophys. J. Int.,* **162,** 221–238, doi:10.1111/j.1365–24X.2005.02608.x.

Kirkwood, B.H., Royer, J.-Y., Chang, T.C. & Gordon, R.G., 1999. Statistical tools for estimating and combining finite rotations and their uncertainties, *Geophys. J. Int.,* **137,** 408–428.

Lemaux, J., Gordon, R.G. & Royer, J.-Y., 2002. The location of the Nubia-Somalia boundary along the Southwest Indian Ridge, *Geology,* **30,** 339–342.

Liu, C.-S., Curray, J.R. & McDonald, J.M., 1983. New constraints on the tectonic evolution of the eastern Indian Ocean, *Earth planet. Sci. Lett.,* **65,** 331–342.

Mart, Y., 1988. The tectonic setting of the Seychelles, Mascarene and Amirante Plateaus in the Western Equatorial Indian Ocean, *Mar. Geol.,* **79,** 261–274.

Masson, D.G., 1984. Evolution of the Mascarene Basin, Western Indian Ocean and the significance of the Amirante arc, *Mar. geophys. Res.,* **6,** 365–382.

McKenzie, D.P. & Sclater, J.G., 1971. The evolution of the Indian Ocean since the Late Cretaceous, *Geophys. J. R. astro. Soc.,* **25,** 437–528.

Miles, P.R., 1982. Gravity models of the Amirante Arc, western Indian Ocean, *Earth planet. Sci. Lett.,* **61,** 127–135.

Molnar, P., Pardo-Casas, F. & Stock, J., 1988. The Cenozoic and Late Cretaceous evolution of the Indian Ocean: uncertainties in the reconstructed positions of the Indian, African and Antarctic plates, *Basin Res.,* **1,** 23–40.

Molnar, P. & Tapponnier, P., 1975. Cenozoic tectonics of Asia: effects of a continental collision, *Science,* **189,** 419–426.

Muller, R.D., Royer, J.-Y., Cande, S.C., Roest, W.R. & Maschenkov, S., 1999. New constraints on the late cretaceous/tertiary plate tectonic evolution of the Caribbean, in *Caribbean Basins, Volume 4: Sedimentary Basins of the World,* pp. 33–59, ed. Mann, P., Elsevier Science, Amsterdam.

Nankivell, A.P., 1997. Tectonic evolution of the southern ocean between Antarctica, South America and Africa over the last 84 Ma, *PhD thesis*, Univ. of Oxford, Oxford, p. 303.

Norton, I.O., 1995. Plate motions in the North Pacific: the 43 Ma nonevent, *Tectonics,* **14,** 1080–1094.

Norton, I.O. & Sclater, J.G., 1979. A model for the evolution of the Indian Ocean and the breakup of Gondwanaland, *J. geophys. Res.,* **84,** 6803–6830.

Patriat, P., 1987. *Reconstitution de l'évolution du système de dorsales de l'océan Indien par les méthodes de la cinématique des plaques,* 308 pp., Territoire des Terres Australes et Antarctiques Françaises, Mission de Recherche, Paris.

Patriat, P. & Achache, J., 1984. India-Eurasia collision chronology has implications for shortening and driving mechanism of plates, *Nature,* **311,** 615–621.

Patriat, P. & Courtillot, V., 1984. On the stability of triple junctions and its relation to episodicity in spreading, *Tectonics,* **3,** 317–332.

Patriat, P. & Segoufin, J., 1988. Reconstruction of the Central Indian Ocean, *Tectonophysics,* **155,** 211–234.

Patriat, P., Segoufin, J., Goslin, J. & Beuzart, P., 1985. Relative positions of Africa and Antarctica in the Upper Cretaceous: evidence for non-stationary behaviour of fracture zones, *Earth planet. Sci. Lett.,* **75,** 204–214.

Patriat, P., Sloan, H. & Sauter, D., 2008. From slow to ultraslow: a previously undetected event at the Southwest Indian Ridge at ca. 24 Ma, *Geology,* **36,** 207–210, doi:10.1130/G24270A.1.

Plummer, P.S., 1996. The Amirante ridge/trough complex: response to rotational transform rift/drift between Seychelles and Madagascar, *Terra Nova,* **8,** 34–47.

Royer, J.Y. & Chang, T., 1991. Evidence for relative plate motions between the Indian and Australian plates during the last 20 m.y. from plate tectonic reconstructions: implications for the deformation of the Indo-Australian plate, *J. geophys. Res.,* **96,** 11 779–11 802.

Royer, J.Y., Chaubey, A.K., Dyment, J., Bhattacharya, G.C., Srinivas, K., Yatheesh, V. & Ramprasad, T., 2002. Paleogene plate tectonic evolution of the Arabian and Eastern Somali basins, in *The Tectonic and Climatic Evolution of the Arabian Sea Region,* pp. 7–23, eds Clift, P.D., Croon, D., Gaedicke, C., Craig, J., Geological Society, London.

Royer, J.-Y. & Gordon, R.G., 1997. The motion and boundary between the Capricorn and Australian plates, *Science,* **277,** 1268–1274.

Royer, J.-Y., Gordon, R.G. & Horner-Johnson, B.C., 2006. Motion of Nubia relative to Antarctica since 11 Ma: implications for Nubia-Somalia, Pacific-North America, and India-Eurasia motion, *Geology,* **34,** 501–504, doi:10.1130/G22463.1.

Royer, J.-Y., Patriat, P., Bergh, H.W. & Scotese, C.R., 1988. Evolution of the southwest Indian Ridge from the late Cretaceous (anomaly 34) to the Middle Eocene (anomaly 20), *Tectonophysics,* **155,** 235–260.

Royer, J.Y. & Sandwell, D.T., 1989. Evolution of the Eastern Indian Ocean since the late Cretaceous: constraints from Geosat altimetry, *J. geophys. Res.,* **94,** 13 755–13 782.

Sandwell, D.T. & Smith, W.H.F., 1997. Marine gravity anomaly from Geosat and ERS-1 satellite altimetry, *J. geophys. Res.,* **102,** 10 039–10 054.

Schlich, R., 1975. Structure et age de l'ocean Indien occidental, *Mem. Hors-Ser. Sot. Geol. Fr.,* **6,** 103 pp.

Schlich R., 1982. The Indian Ocean: aseismic ridges, spreading centers and basins, in *The Ocean Basins and Margins,* eds Nairn, A.E., Stehli, F.G., Plenum, New York, pp. 51–147.

Sclater, J.G. & Fisher, R.L., 1974. Evolution of the east central Indian Ocean, with emphasis on the tectonic setting of the Ninetyeast Ridge, *Geol. Soc. Am. Bull.,* **85,** 683–702.

Sclater, J.G., Grindlay, N.R., Madsen, J.A. & Rommevaus-Jestin, C., 2005, Tectonic interpretation of the Andrew Bain transform fault: southwest Indian Ocean, *Geochem. Geophys. Geosys.,* **6,** doi:10.1029/2005GC000951.

Sclater, J.G., Munschy, M., Fisher, R.L., Weatherall, P.A., Cande, S.C., Patriat, P., Bergh, H. & Schlich, R., 1997. Geophysical synthesis of the Indian/Southern Oceans. Part 1, The southwest Indian Ocean, SIO Ref. Ser. 97–06: San Diego, La Jolla, Scripps Institute. of Oceanography, Univ. of Calif., p. 45.

Sharp, W.D. & Clague, D.A., 2006. 50 Ma Hawaiian: emperor bend records major change in Pacific plate motion, *Science,* **313,** 1281–1284.

Shaw, P.R. & Cande, S.C., 1990. High-resolution inversion for South-Atlantic plate kinematics using joint altimeter and magnetic data, *J. geophys. Res.,* **95,** 2625–2644.

Stephens, W.E., Storey, M., Donaldson, C.H., Ellam, R.M., Lelikov, E., Tararin, G. & Garbe-Schoenberg, C., 2009. Age and origin of the Amirante ridge-trench structure, western Indian Ocean, Fall 2009 AGU [abstract] T23A-1885.

Tararin, I.A. & Lelikov, E.P., 2000. Amirante island arc in the Indian Ocean: data on the initial island arc magmatism, *Petrology,* **8,** 53–65.

Todal, A. & Eldholm, O., 1998. Continental margin off Western India and Deccan large igneous province. *Mar. geophys. Res.*, **20,** 273–291.

Whittaker, J.M., Müller, R.D., Leitchenkov, G., Stagg, H., Sdrolias, M., Gaina, C. & Goncharov, A., 2007. Major Australian-Antarctic plate reorganization at Hawaiian-Emperor bend time, *Science,* **318,** 83–86.

Wiens, D.A. *et al*., 1985. A diffuse plate boundary model for Indian Ocean tectonics, *Geophys. Res. Lett.,* **12,** 429–432.

Yatheesh, V, Bhattacharya, G.C. & Dyment, J., 2009. Early oceanic opening off western India-Pakistan margin: the Gop Basin revisited, *Earth planet. Sci. Lett.,* **284,** 399–408.

APPENDIX A: EFFECT OF MOTION BETWEEN THE SOMALIA, NUBIA AND LWANDLE PLATES

We investigated the effects of correcting data constraints on the SWIR for the small amounts of motion between the Nubia, Somalia and Lwandle plates as prescribed by the rotations of Horner-Johnson *et al*. (2007). Specifically, we corrected (i.e. rotated back to their original position relative to the Somali Plate) the constraints on the African Plate from west of the Bain fracture zone by the Nubia–Somalia rotation (lat. = 37.0°S, long. = 27.1°E, delta = –0.2944°) and from between the Prince Edward fracture

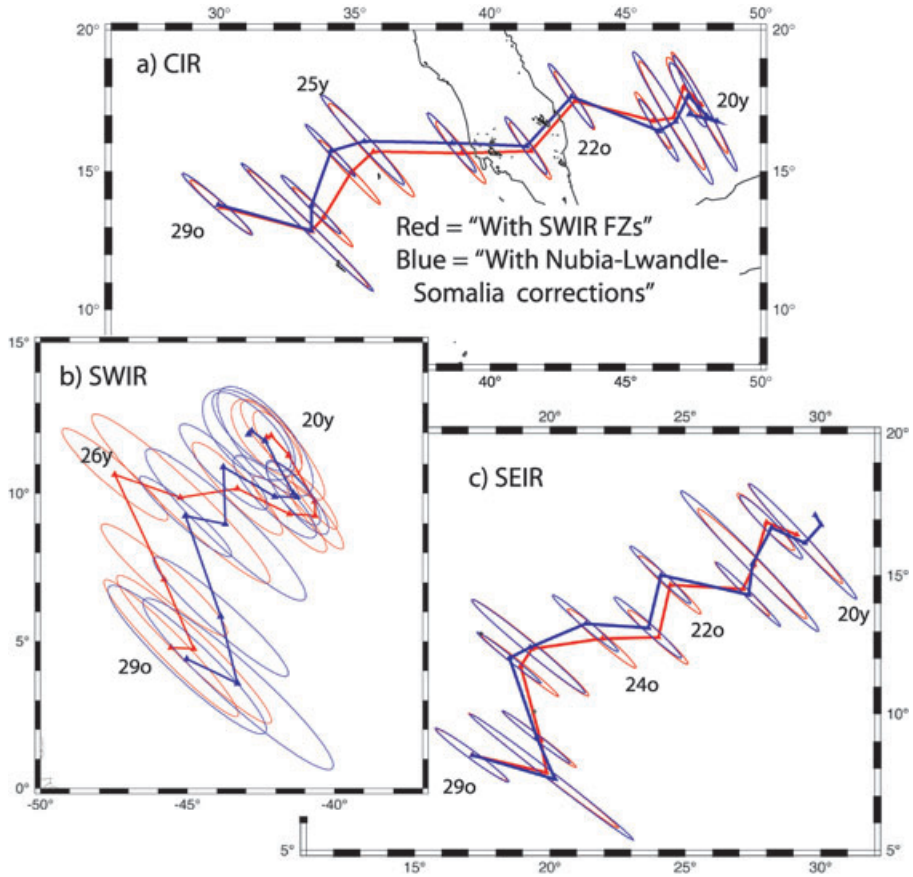

Figure A1. Comparison of Euler poles constrained with data set 2 ('With SWIR FZs', red) to Euler poles constrained with corrections for Nubia–Somalia and Lwandle–Somalia motion (blue). Note the relatively small effect of these corrections on the Euler poles.

zone and Simpson fracture zone by the Lwandle–Somalia rotation (lat. = 27.8°S, long. = 52.2°E, delta = –0.2122°). Because the boundary between the Lwandle and Nubia plates may intersect the SWIR near the Bain fracture zone, we dropped the constraints from the three fracture zone splays within the Bain fracture zone itself and only kept constraints from the two fracture zones west of the Bain (the DuToit and an unnamed one). For the constraints west of the Bain FZ the effect of the correction is to shift the data points about 10 km to the west while for the constraints between the Prince Edward and Simpson FZs the effect is to shift the points about 7 km to the northwest. We then reran the solutions for data set 2 ('With SWIR FZs'). The results ('With Nubia') are shown in Fig. A1 and given in Table A1. The differences between the rotations with and without the corrections are all relatively small, particularly for the CIR and SEIR rotations. Because there is some uncertainty in the extent of the various diffuse plate boundaries along the SWIR, we decided not to include corrections for these small rotations in our study.

Table A1. Finite rotations for data set 2 with corrections for Lwandle–Nubia–Somalia motion.

Anom	Lat. (°N)	Long. (°E)	Angle (°)	$\hat{\kappa}$	a	b	c	d	e	f	Points	Segs
						Capricorn–Antarctica						
20y	−16.16	−150.58	24.76	0.83	14.69	66.15	314.06	−23.29	−111.41	41.41	105	14
20o	−16.71	−151.81	25.23	0.71	3.39	15.84	88.14	−5.33	−29.64	11.68	131	14
21y	−15.43	−152.51	26.80	0.55	16.14	75.01	361.50	−25.21	−121.12	42.77	105	12
21o	−14.31	−152.65	28.24	1.68	12.73	59.54	290.58	−19.03	−92.82	31.21	114	12
22o	−15.01	−155.90	29.40	1.40	12.00	55.99	272.34	−17.35	−84.40	28.80	113	12
23o	−13.12	−156.36	32.33	0.85	7.49	34.15	166.61	−9.49	−46.23	14.51	118	13
24o	−13.27	−158.67	34.31	1.10	11.31	51.08	244.26	−12.85	−61.19	17.32	98	12
25y	−12.42	−160.74	37.47	0.64	22.24	100.05	468.58	−22.16	−103.88	25.56	74	11
26y	−12.04	−161.49	39.50	2.32	23.44	108.76	524.46	−21.64	−104.63	23.04	75	10
27y	−9.15	−160.49	44.11	1.25	23.65	111.41	541.58	−17.72	−86.96	16.09	78	11
28y	−7.61	−159.81	46.65	0.60	80.83	342.40	1477.96	−49.95	−216.48	33.72	73	11
29o	−8.49	−162.86	49.05	0.49	10.34	50.67	271.25	−5.69	−31.67	5.74	83	13
						Capricorn–Somalia						
20y	−16.97	−132.00	23.26	0.83	22.80	82.72	309.77	−24.44	−91.62	28.27	105	14
20o	−17.69	−132.67	23.51	0.71	5.82	21.12	83.19	−6.31	−23.52	8.34	131	14
21y	−16.77	−133.16	24.83	0.55	21.84	83.18	326.84	−23.22	−90.27	26.47	105	12
21o	−16.44	−133.75	26.08	1.68	16.43	63.65	253.30	−16.57	−64.99	18.44	114	12
22o	−17.66	−136.99	26.61	1.40	15.26	58.50	231.97	−14.64	−57.59	16.04	113	12
23o	−15.90	−138.66	29.42	0.85	10.19	37.76	144.51	−9.04	−34.26	9.73	118	13
24o	−16.01	−141.40	31.12	1.10	14.58	55.07	214.98	−12.02	−46.14	11.83	98	12
25y	−16.07	−144.65	33.78	0.64	24.77	94.85	375.27	−17.47	−68.28	14.59	74	11
26y	−15.73	−145.88	35.77	2.32	27.98	114.08	481.91	−20.05	−84.51	16.89	75	10
27y	−13.79	−146.59	40.23	1.25	29.08	118.14	498.44	−17.22	−72.41	12.80	78	11
28y	−12.88	−146.61	42.70	0.60	82.79	328.65	1324.98	−42.45	−171.68	24.26	73	11
29o	−13.80	−150.04	44.67	0.49	14.58	60.33	266.39	−5.75	−25.02	4.08	83	13
						Antarctica–Somalia						
20y	11.96	−42.92	7.53	0.83	3.69	3.24	4.13	−2.33	−3.78	8.67	105	14
20o	12.07	−42.81	7.88	0.71	2.33	2.06	3.15	−2.28	−3.51	6.38	131	14
21y	11.74	−42.36	8.52	0.55	2.81	2.66	4.01	−3.12	−5.05	10.76	105	12
21o	10.00	−41.40	8.84	1.68	2.85	2.79	4.11	−4.11	−5.60	11.99	114	12
22o	9.88	−41.27	9.25	1.40	3.29	3.41	5.27	−5.37	−7.34	15.17	113	12
23o	9.89	−42.03	9.65	0.85	3.82	4.02	6.23	−5.59	−7.47	12.69	118	13
24o	10.89	−43.78	10.01	1.10	6.32	6.39	8.73	−9.35	−11.09	18.74	98	12
25y	8.97	−43.71	10.43	0.64	11.39	13.37	18.66	−18.88	−24.55	37.76	74	11
26y	9.24	−45.07	10.69	2.32	15.07	17.57	22.43	−23.44	−29.07	42.21	75	10
27y	5.85	−43.87	11.02	1.25	18.36	21.00	27.34	−28.95	−35.11	51.47	78	11
28y	3.58	−43.30	11.33	0.60	18.28	21.48	28.31	−29.67	−36.54	54.07	73	11
29o	4.40	−45.02	11.68	0.49	11.87	12.89	15.92	−18.90	−21.84	35.34	83	13